

# Hierarchy of Entanglement Renormalization and Long-Range Entangled States

Meng-Yuan Li and Peng Ye\*

*School of Physics, State Key Laboratory of Optoelectronic Materials and Technologies,  
and Guangdong Provincial Key Laboratory of Magnetoelectric Physics and Devices, Sun Yat-sen University, Guangzhou, 510275, China*  
(Dated: Monday 21<sup>st</sup> October, 2024)

As a quantum-informative window into condensed matter physics, the concept and application of entanglement renormalization group (ERG) have been playing a vital role in the study of novel quantum phases of matter, especially topologically ordered phases that exhibit long range entanglement (LRE) patterns. For instance, by recursively applying local unitaries as well as adding/removing qubits that form product states, the 2D toric code ground states, i.e., fixed point of  $\mathbb{Z}_2$  topological order, are efficiently coarse-grained with respect to the system size. Recently, in an improved ERG framework, the addition/removal of 2D toric codes into/from the ground states of the 3D X-cube model, is shown to be indispensable and remarkably leads to well-defined fixed points of a large class of fracton orders. Here, we find that such progress of ERG is not the end of story if more general degrees of freedom are allowed to be added/removed. Specifically, we establish an interesting hierarchy structure of ERG and LRE states in a class of Pauli stabilizer codes, where the 2D toric code and 3D X-cube model are naturally included. In the hierarchy, LRE states like both 3D X-cube and 3D toric code ground states can be added/removed in an ERG process of more complex LRE states. In this way, all Pauli stabilizer codes considered here are categorized into a series of “state towers”; in each tower, lower LRE states of level- $n$  are added/removed in the level- $n$  ERG process of an upper LRE state of level- $(n+1)$ , which builds bridges between LRE states of different levels. As future directions, we expect this hierarchy can be further generalized in more exactly solvable models. We also expect the resulting fixed points may admit tensor-network representation in the form of more generalized exact branching MERA.

## I. INTRODUCTION

For the past decades, the goal of classification and characterization of novel quantum phases of matter has been indispensably intertwined with the surprisingly rapid progress on many-body quantum entanglement [1–16]. This line of efforts significantly reshapes modern many-body physics from the emphasis of entanglement structure instead of local correlation functions and local order parameters. For instance, the topologically ordered ground states of, e.g., fractional quantum Hall liquids [17], chiral spin liquids [18], the toric code [19, 20] and string-net models [21] have been identified as long-range entangled (LRE) states [9] that cannot be adiabatically connected to (unentangled) product states by local unitary (LU) transformations, i.e., disentanglers. In contrast, short-range entangled states (SRE) can always be connected to product states by LU transformations. In particular, symmetry protected topological states (SPT), e.g., the Haldane spin chain, are a special class of SRE states in which all above-mentioned LU transformations inevitably break the global symmetry that protects SPT order. Remarkably, a series of stabilizer code models realizing topological orders are found to be fixed points of certain entanglement renormalization group (ERG) transformations [4, 5, 7] that simultaneously lead to an efficient representation of the topologically ordered ground state in terms of a tensor network, the multiscale entanglement renormalization ansatz (MERA) [6–8]. The idea of ERG provides a remarkable quantum-informative framework that significantly revolutionizes the traditional real-space and momentum-space renormalization-group treatments of quantum many-body systems and quantum field theory. More

specifically, during the process of ERG transformations, LU transformations and addition/removal of product states are recursively performed, such that the number of qubits (i.e., the system size) and short-range entanglement can be coarse-grained while the long-range entanglement patterns (e.g., braiding and fusion data of 2D anyon systems) keep unaltered. Such LU transformations combined with addition/removal of product states are also dubbed generalized local unitary (gLU) transformations [9].

Recently, a significant improvement of ERG transformations has been made in order to quantum-informatively identify fixed points of *fracton orders*—an exotic class of topologically ordered non-liquids [22–30], which broadens our understandings on entanglement structures of LRE states. In contrast to the pure topological orders (e.g., the fractional quantum Hall states) that are liquid states, fracton orders are a kind of non-liquid LRE states whose local Hamiltonians support ground state degeneracy (GSD) that not only is locally indistinguishable but also grows subextensively with respect to the system size. For example, the GSD of X-cube model—the prototypical example of type-I fracton order—on a 3-torus satisfies that  $\log_2 GSD$  grows linearly with the linear system size  $L$  [31]. Later, it has been discovered that, to consistently define quantum phases and fixed points of fracton orders under entanglement renormalization, not only product states, but also pure topological orders defined on lower dimensional space should be added/removed, such that two fracton-ordered states of different system sizes are connected [22]. Such an idea of ERG improvement is really intriguing, which motivates us to explore a potentially unified ERG framework of LRE states through, e.g., considering addition/removal of more general lower-dimensional degrees of freedom.

In this paper, we attempt to provide a hierarchical structure of ERG as well as the associated LRE states, where the

\* yepeng5@mail.sysu.edu.cn

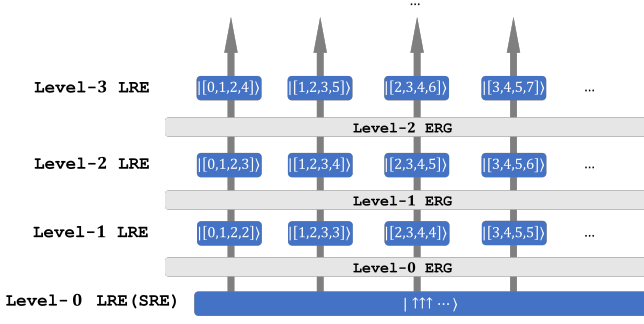


FIG. 1. **Illustration of state towers that exhibit a hierarchy of entanglement renormalization and long-range entangled states.** For concreteness, a class of Pauli stabilizer codes [32, 33] are studied.  $[D-2, D-1, D, D]$  denotes pure  $\mathbb{Z}_2$  topologically ordered models.  $[0, 1, 2, 2]$ ,  $[1, 2, 3, 3]$  and  $[0, 1, 2, 3]$  are respectively 2D toric code, 3D toric code and 3D X-cube models,  $|\cdot\rangle$  refers to a ground state of a certain model (i.e., a state in the stabilizer subspace, see Sec. II). There are a series of state towers denoted by upward arrows, and along each arrow, a lower  $\text{LRE}^n$  state can be added/removed in the  $\text{ERG}^n$  process of the upper  $\text{LRE}^{n+1}$  state as demonstrated in Eq. (1). To unify the notation, SRE states are symbolically denoted as  $\text{LRE}^0$ .

above ERG transformations of original definition [4, 5, 7] and that of X-cube model [22] are naturally included and substantially generalized. To be more specific, as shown in Fig. 1, we construct ERG transformations for a series of Pauli stabilizer code models[34] proposed in Ref. [32], such that the models are fixed points of ERG transformations. All models we will study in this paper are uniquely denoted by four integers, i.e.,  $[d_n, d_s, d_l, D]$ , where a subset labeled by  $[d, d+1, d+2, D]$  is found to be Pauli stabilizer code models with emergent  $\mathbb{Z}_2$  gauge symmetry (see Sec. II for more details). The familiar 3D X-cube and 2D toric code models are respectively denoted as  $[0, 1, 2, 3]$  and  $[0, 1, 2, 2]$ . Remarkably, in the ERG transformations of these Pauli stabilizer codes, we find a hierarchical structure summarized in Fig. 1: in an ERG transformation connecting two  $[d, d+1, d+2, D]$  states (i.e., the ground states of  $[d, d+1, d+2, D]$  model as lattice Hamiltonian) of different sizes,  $[d, d+1, d+2, D-1]$  states can be added/removed, such that all Pauli stabilizer codes are fixed-point Hamiltonians under ERG transformations. While the  $\log_2 \text{GSD}$  of these topological non-liquid models grows polynomially with respect to the linear system size [33], ERG transformations keep the GSD formulas consistent in different length scales. All in all, the ERG relation can be symbolically expressed as follows:  $|\![d, d+1, d+2, D]\rangle \sim |\![d, d+1, d+2, D]\rangle' \otimes [d, d+1, d+2, D-1]$ , where  $|\![d, d+1, d+2, D]\rangle$  and  $|\![d, d+1, d+2, D]\rangle'$  are  $[d, d+1, d+2, D]$  states of different sizes, and  $\sim$  means the two sides can be connected by an LU transformation. More concretely, ERG transformations obey the following recursive rules:

- In the ERG transformations on Pauli stabilizer codes considered here, LRE states are categorized into different levels, denoted as  $\text{LRE}^n$  with the level index  $n = 0, 1, 2, \dots$ . Unentangled product states and more general SRE states are dubbed “level-0 LRE states” (de-

noted as  $\text{LRE}^0$  symbolically);

- ERG transformations where level- $n$  LRE states are added/removed are dubbed “level- $n$  ERG” (denoted as  $\text{ERG}^n$  symbolically) transformations. Unless otherwise specified,  $n$  is the highest level of add/removed LRE states;
- States of the same stabilizer code with different sizes that can be connected by level- $n$  ERG transformations are identified as  $\text{LRE}^{n+1}$ .

Then an  $\text{ERG}^n$  transformation can be symbolically expressed as follows:

$$\text{ERG}^n : \text{LRE}^{n+1} \sim \text{LRE}^{n+1} \otimes \text{LRE}^n \quad (1)$$

which explicitly shows a hierarchy of ERG transformations as well as LRE states along each upward arrow in Fig. 1. For example, the ERG of the 2D toric code is given by  $\text{ERG}^0$  [4, 5, 7, 14]:

$$\text{ERG}^0 : \text{LRE}^1 \sim \text{LRE}^1 \otimes \text{LRE}^0, \quad (2)$$

where a toric code ground state denoted as  $\text{LRE}^1$  and product states denoted as  $\text{LRE}^0$  are added/removed (note that SRE states are also denoted as  $\text{LRE}^0$ ). Similarly, the ERG of the 3D X-cube model is given by  $\text{ERG}^1$  [22]:

$$\text{ERG}^1 : \text{LRE}^2 \sim \text{LRE}^2 \otimes \text{LRE}^1, \quad (3)$$

where an X-cube ground state is denoted as  $\text{LRE}^2$  and the 2D toric code ground state  $\text{LRE}^1$  is added/removed. In fact, Eq. (1) may be a concrete realization of the following possibly exist more general level- $m$  ERG transformation denoted as  $\text{ERG}^m$ :

$$\text{ERG}^m : \text{LRE}^n \sim \text{LRE}^n \otimes \text{LRE}^m, \quad (4)$$

where  $m < n$  is generally required. We leave such general ERG transformations as well as implied MERAs to further exploration.

The remainder of this paper is organized as follows. In Sec. II, we introduce some geometric notations used in this paper and give a brief introduction to the  $[d, d+1, d+2, D]$  models, which include toric code and X-cube models. Sec. III is dedicated to a detailed demonstration of some concrete ERG transformations. In Sec. III A and Sec. III B, we respectively review the ERG transformations of the 2D toric code model and the 3D X-cube model (respectively denoted as  $[0, 1, 2, 2]$  and  $[0, 1, 2, 3]$  models in this paper). Then, we concretely construct the ERG transformations of different levels for  $[0, 1, 2, 4]$ ,  $[1, 2, 3, 4]$  models respectively in Sec. III C, III D. Sec. IV is dedicated to a discussion about ERG transformations for general  $[d, d+1, d+2, D]$  models. In Sec. IV A, we demonstrate a general recipe for the ERG transformations of general  $[d, d+1, d+2, D]$  models, and prove that the models are indeed fixed points of corresponding ERG transformations in Sec. IV B. After that, we demonstrate how these ERG transformations lead to the concept of a hierarchy of ERG transformations and LRE states in Sec. IV C. Finally, in Sec. V we discuss about some possible directions of further studies.

## II. GEOMETRIC NOTATIONS AND PAULI STABILIZER CODES

This section is dedicated to the introduction of some backgrounds, including geometric notations and a family of Pauli stabilizer code models denoted by  $[d, d+1, d+2, D]$ . Specially, we noticed that  $[D-2, D-1, D, D]$  model can be regarded as a  $D$ -dimensional generalization of toric code model.

In this paper we need to involve some discussion about high dimensional geometric objects, so we believe it is beneficial to at first introduce some relevant notations. For a hypercubic lattice discussed in this paper, unless otherwise specified, we set lattice constant to be 1. Then, we introduce the concept of  $n$ -cubes denoted by  $\gamma_n$ , that simply refers to  $n$ -dimensional analogs of cube. For example, a  $\gamma_0$  (0-cube) is simply a vertex, a  $\gamma_1$  (1-cube) is a link, a  $\gamma_2$  (2-cube) is a plaquette and a  $\gamma_3$  (3-cube) is a conventional cube. In a  $D$ -dimensional hypercubic lattice, with the above notations, we can use the coordinates of the center of a  $\gamma_n$  ( $n < D$  is assumed) to refer to the  $\gamma_n$  itself, as such a  $\gamma_n$  can be uniquely determined by the coordinates. Besides, we can see that the coordinate representation of a  $\gamma_n$  in a  $D$ -dimensional hypercubic lattice is always composed of  $n$  half-odd-integers (or half-integer in shorthand) and  $(D-n)$  integers. For example, in 3D cubic lattice, the coordinate representation of a  $\gamma_2$  (i.e. plaquette), such as  $(\frac{1}{2}, \frac{1}{2}, 0)$  and  $(\frac{7}{2}, 5, \frac{1}{2})$ , always contains 2 half-integers and 1 integer. What's more, following the terminology in Ref. [32], we say a  $n$ -cube  $\gamma_n = (x_1, x_2, \dots, x_D)$  and a  $m$ -cube  $\gamma_m = (y_1, y_2, \dots, y_D)$  to be nearest to each other when  $|x_1 - y_1| + |x_2 - y_2| + \dots + |x_D - y_D| = \frac{|m-n|}{2}$  for  $m \neq n$ . Specially, when  $m = n$ , we say they are nearest to each other when  $|x_1 - y_1| + |x_2 - y_2| + \dots + |x_D - y_D| = 1$ . We can check that such a definition of being nearest is consistent with the usual conventions.

Next, we give a brief review to the definition of  $[d, d+1, d+2, D]$  Pauli stabilizer code models. As lattice Hamiltonians,  $[d, d+1, d+2, D]$  models is a subset of  $[d_n, d_s, d_l, D]$  models proposed in Ref. [32]. In general, a  $[d_n, d_s, d_l, D]$  model is defined on a  $D$ -dimensional hypercubic lattice, with one  $\frac{1}{2}$ -spin defined on each  $d_s$ -cube (i.e.  $\gamma_{d_s}$ ). And the Hamiltonian is given as follows:

$$H_{[d_n, d_s, d_l, D]} = - \sum_{\gamma_D} A_{\gamma_D} - \sum_{\gamma_{d_n}} \sum_l B_{\gamma_{d_n}}^l, \quad (5)$$

where a  $B_{\gamma_{d_n}}^l$  term is the product of the  $z$ -components of the spins (a) being nearest to the  $d_n$ -cube  $\gamma_{d_n}$  and (b) living in a  $d_l$ -dimensional subsystem given by index  $l$ , and an  $A_{\gamma_D}$  term is the product of the  $x$ -components of the spins being nearest to the  $D$ -cube  $\gamma_D$ . Here for simplicity, all coefficients of terms have been set to be  $-1$ . A concrete example of the Hamiltonian of  $[0, 1, 2, 3]$  (a.k.a. X-cube) model is illustrated in Fig. 2(b). In Ref. [32]  $d_n < d_s < d_l < D$  is assumed, while in this paper, we allow the case  $d_l = D$  for reasons to be discussed in the following part.

In this paper we focus on  $[d, d+1, d+2, D]$  models (i.e., where we set  $d_n = d$ ,  $d_s = d+1$ ,  $d_l = d+2$ ). Here, we noticed that 2D and 3D toric code models can be recognized

as  $[0, 1, 2, 2]$  and  $[1, 2, 3, 3]$  models respectively. Because they do not satisfy the  $d_l < D$  condition, now the superscripts of  $B$  terms are redundant, and a  $B_{\gamma_d}$  term is simply the product of the  $z$ -components of the 4 spins nearest to the  $\gamma_d$ . Such models are not fracton ordered, thus they were less involved in Ref. [32]. Nevertheless, to give a more systematic demonstration of the hierarchy of ERG transformations, in this paper it is convenient to recognize such a  $[D-2, D-1, D, D]$  model as a  $D$ -dimensional generalization of toric code model, and add  $[D-2, D-1, D, D]$  models into the family of  $[d, d+1, d+2, D]$  models as in Fig. 1.

To see the equivalence between the  $[D-2, D-1, D, D]$  model and a  $D$ -dimensional toric code model, we only need to consider a duality, where  $\gamma_n$ 's are mapped to  $\gamma_{D-n}$ 's, that can be concretely realized by adding  $(\frac{1}{2}, \frac{1}{2}, \dots, \frac{1}{2})$  to the coordinates of all  $\gamma_n$ 's. After that, the  $[D-2, D-1, D, D]$  model is still defined on a  $D$ -dimensional hypercubic lattice, but now with one  $\frac{1}{2}$ -spin defined on each 1-cube (a.k.a. link), and the Hamiltonian is given by  $H_{dual} = - \sum_v A_v - \sum_p B_p$ , where  $A_v$  is the product of  $x$ -components of spins nearest to the vertex  $v$ ,  $B_p$  is the product of  $z$ -components of spins nearest to the plaquette  $p$ . Such a Hamiltonian is obviously a  $D$ -dimensional generalization of toric code model[35]. Therefore, it is straightforward to check that  $[D-2, D-1, D, D]$  models with  $D \geq 2$  are pure topologically ordered, thus the ground states are LRE<sup>1</sup> states regardless of  $D$ .

Then, we can use a general recipe to obtain the ground states of  $[d, d+1, d+2, D]$  stabilizer code models (including  $[D-2, D-1, D, D]$  models, such as 2D and 3D toric code). The lattice Hamiltonians of these models are all of the following form:

$$H = - \sum_i A_i - \sum_j B_j, \quad (6)$$

where  $i$  and  $j$  are some kinds of spatial locations (e.g. vertices, centers of links, centers of plaquettes) depending on the specific model, and the index  $l$  in Eq. 5 has been formally absorbed into index  $j$  for simplicity. Here,  $A_i$  and  $B_j$  are respectively local products of  $\sigma^x$  and  $\sigma^z$  Pauli operators, and they all commute with each other (see Fig. 2 for examples of 2D toric code and 3D X-cube models). Therefore, a ground state  $|\phi\rangle$  of such a Hamiltonian has to satisfy conditions  $A_i|\phi\rangle = |\phi\rangle$ ,  $\forall i$  and  $B_j|\phi\rangle = |\phi\rangle$ ,  $\forall j$  (respectively denoted as  $A$  and  $B$  constraints). That is to say, for a given  $[d, d+1, d+2, D]$  model, the  $A_i$  and  $B_j$  operators can be regarded as generators of a stabilizer group, and the ground state subspace is the corresponding stabilizer subspace[14, 34], as ground states are ‘‘stabilized’’ by all  $A_i$  and  $B_j$  operators. In this paper, as we mainly care about the stabilizer subspaces, unless otherwise specified, for a given model, we only consider states in its ground state subspace. Then, for an arbitrary  $[d, d+1, d+2, D]$  stabilizer code model, we can obtain a ground state  $|\phi\rangle$  of it by the following procedures:

- First, we consider  $\sigma^z$  basis, that is to say, we use Ising configurations, where spins are denoted by their direction along  $\sigma^z$ , as a basis of the whole Hilbert space. For a single qubit, we use the convention  $\sigma^z|\uparrow\rangle = |\uparrow\rangle =$

$|0\rangle = \begin{pmatrix} 1 \\ 0 \end{pmatrix}$ ,  $\sigma^z|\downarrow\rangle = -|\downarrow\rangle = -|1\rangle = -\begin{pmatrix} 0 \\ 1 \end{pmatrix}$  (i.e.,  $|0\rangle$  for spin up, and  $|1\rangle$  for spin down).

- Then, we can notice that  $|0 \cdots 00\rangle$  naturally satisfies all  $B$  constraints. We denote  $|0 \cdots 00\rangle$  as the reference state.
- Third, we consider the equal weight superposition of the reference state and all configurations that can be obtained by applying a series of  $A_i$  operators on the reference state, and denote this state as  $|\phi\rangle$ . As all  $A_i$  and  $B_j$  operators commute with each other,  $|\phi\rangle$  also satisfies  $B$  constraints. According to our construction of  $|\phi\rangle$ , where 2 configurations that can be related by the action of  $A_i$  are always equally superpositioned, we can see that  $|\phi\rangle$  must also satisfy  $A$  constraints. Hence,  $|\phi\rangle$  is a ground state of the stabilizer code model.

In the following part of this paper, we use an intuitive picture to describe an Ising configuration, by recognizing flipped spins (i.e. spin of the state  $|1\rangle$ ) as occupied by certain geometric objects. For example, if the spins are defined on links, then we recognize flipped spins as occupied by strings; and if the spins are defined on plaquettes, then we recognize flipped spins as occupied by membranes. Consequently, we can denote the  $|\phi\rangle$  obtained by steps above as the no-string ground state (or no-string state in shorthand) for simplicity, despite that not in all cases the spins are defined on links. For a  $[d, d+1, d+2, D]$  model, other ground states can be obtained by applying logical operators on the no-string state. Here in the  $\sigma^z$  basis, a logical operator can be recognized as a product of a series of  $\sigma^x$  operators, that commutes with all  $B_j$  terms and do not equivalent to any product of a series of  $A_i$  terms.

Following this general recipe, we can see that when we ignore the topological degeneracy by focusing on the open boundary condition, we only need to consider the no-string state, that can be regarded as a superposition of a series of configurations. For the no-string state,  $B$  terms require a superpositioned configuration to satisfy certain constraints, like flipped spins forming closed strings in  $[0, 1, 2, 2]$  model;  $A$  terms require configurations that can be connected by action of  $A$  terms to be equal-weight superpositioned. In Sec. III, a series of concrete examples are demonstrated in the corresponding subsections.

### III. HIERARCHY OF ERG TRANSFORMATIONS AND LRE STATES

In this section, we concretely demonstrate the ERG transformations of some concrete  $[d, d+1, d+2, D]$  states (including  $[0, 1, 2, 2]$  states). At first, in Sec. III A and Sec. III B, we give a brief review of the ERG transformations of 2D toric code ( $[0, 1, 2, 2]$ ) and 3D X-cube ( $[0, 1, 2, 3]$ ) models respectively. Then, in Sec. III C and Sec. III D, we respectively construct the ERG transformations for  $[0, 1, 2, 4]$  and  $[1, 2, 3, 4]$  models.

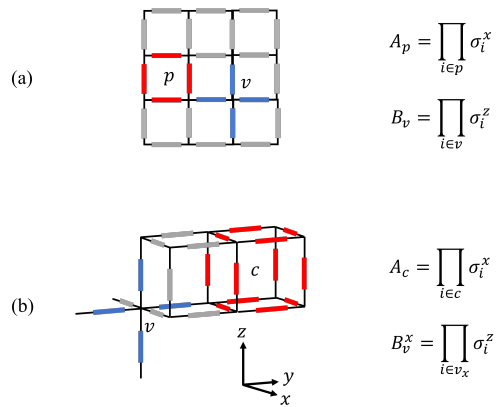


FIG. 2. **Hamiltonians of some representative  $[d, d+1, d+2, D]$  models.** (a) and (b) respectively demonstrate the Hamiltonian terms of the  $[0, 1, 2, 2]$  (2D toric code) and the  $[0, 1, 2, 3]$  (3D X-cube) model. In each subfigure, spins are represented by bars on links, and we draw spins acted by an  $A$  term with red, and spins acted by a  $B$  term with blue. In (b), we only draw a single  $B_v^x$  term on vertex  $v$ , that is composed of the 4 spins that are not only nearest to vertex  $v$  but also located in a plane perpendicular to  $x$ -direction. Such 4 spins are denoted as  $i \in v_x$  in (b).

#### A. Level-0 ERG transformation of $[0, 1, 2, 2]$ (2D toric code) states

Here, we review the ERG<sup>0</sup> transformation of  $[0, 1, 2, 2]$  states following the recipe in Ref. [14]. At first, we give an intuitive picture of the  $[0, 1, 2, 2]$  states based on the general discussion in Sec. II. In  $[0, 1, 2, 2]$  (a.k.a. 2D toric code) model, spins are located at links of a 2D square lattice. In a superpositioned configuration of a  $[0, 1, 2, 2]$  state, a  $B_j$  term requires vertex  $j$  can only have 0, 2 or 4 flipped nearest spins, thus flipped spins must form closed strings. An  $A_i$  term flips the 4 spins on the links of plaquette  $i$ , thus contractible closed strings can freely fluctuate in a ground state. We will see that, the ERG transformation indeed preserves this closed strings pattern of  $[0, 1, 2, 2]$  states.

In the ERG<sup>0</sup> transformation of a 2D toric code ground state defined on a square lattice with periodic boundary condition (PBC), we firstly separate vertices into A and B sublattices. Then, we put an additional  $1/2$ -spin in state  $|0\rangle$  on each vertex (see Fig. 3(a)). After that, we apply an LU transformation  $\mathcal{U}_1$ , that is composed of a series of CNOT (controlled-NOT) gates: for each additional spin, we act two CNOT gates targeting on it. More specifically, for an additional qubit in sublattice A, we use the qubits on the up and left links as control qubits; for an additional qubit in sublattice B, we use qubits on the up and right links (see Fig. 3(b)). The action of  $\mathcal{U}_1$  can be understood pictorially: recall that in any allowed Ising configuration of a toric code ground state there must be either even or zero number of  $|1\rangle$  spins around each vertex, thus flipped spins always form closed strings. Then, we can notice that the design of CNOT gates in  $\mathcal{U}_1$  exactly preserves this constraint by integrating additional spins into the closed strings pattern.

After that, we further apply an LU transformation  $\mathcal{U}_2$  to map the spins around each square to  $|0000\rangle + |1111\rangle$  (normal-

ization is omitted), and such spins can be removed out of the state as  $|0000\rangle + |1111\rangle$  can be transformed to a product state by a local unitary operator. For the lattice, the LU transformation  $\mathcal{U}_2$  effectively shrinks every square to a vertex as shown in Fig. 3(c). By noticing that in each configuration there is always 0 or an even number of diagonal links around each square with qubits in  $|1\rangle$ , the resulting state also has the closed strings pattern. Here, to see that  $\mathcal{U}_2$  is indeed an LU transformation, we can recognize  $\mathcal{U}_2 = \prod_s \mathcal{U}_s$ , which is the product of  $\mathcal{U}_s$  operators supported around each square  $s$ . A  $\mathcal{U}_s$  acts on the four qubits on links nearest to the square  $s$  (denoted by  $i, j, k$  and  $l$ ) and the four qubits on the diagonal links around  $s$  (denoted by  $a, b, c$  and  $d$ , see Fig. 3(d)). Here,  $\mathcal{U}_s$  can be roughly recognized as a generalized CNOT gate: it takes the qubits on diagonal links as control qubits, and qubits on the square as targets. For a specific configuration of the eight qubits, the action of  $\mathcal{U}_s$  can be obtained as follows: a) if all control qubits are  $|0\rangle$ , then flip no target qubits; b) if two control qubits are  $|1\rangle$ , then flip the target qubits between them clockwise following the alphabetical order (e.g. if qubits on  $b$  and  $d$  are  $|1\rangle$ , then flip qubits on  $j$  and  $k$ ); c) if all control qubits are in  $|1\rangle$ , then flip qubits on  $i$  and  $k$ . Then,  $\mathcal{U}_s$  obviously satisfies  $\mathcal{U}_s \mathcal{U}_s = \mathbb{I}$ , thus  $\mathcal{U}_s^{-1} = \mathcal{U}_s$ . Next, notice that Ising configurations form a complete basis of the Hilbert space, for an arbitrary pair of Ising configurations of the eight qubits  $|\psi_1\rangle$  and  $|\psi_2\rangle$ , we can obtain that  $\langle \psi_1 | \mathcal{U}_s | \psi_2 \rangle = \langle \psi_2 | \mathcal{U}_s | \psi_1 \rangle^*$ : we only have  $\langle \psi_1 | \mathcal{U}_s | \psi_2 \rangle = 1$  when the control qubits in  $|\psi_1\rangle$  and  $|\psi_2\rangle$  are all the same, and only the qubits to be flipped are different in  $|\psi_1\rangle$  and  $|\psi_2\rangle$ ; otherwise,  $\langle \psi_1 | \mathcal{U}_s | \psi_2 \rangle = 0$ . As a result,  $\mathcal{U}_s^\dagger = \mathcal{U}_s = \mathcal{U}_s^{-1}$ , thus  $\mathcal{U}_s$  is both unitary and Hermitian. Since the transformations above do not change the pattern that the state is invariant under the action of  $A_p$  terms on squares, and  $\mathcal{U}_s$  always maps the configuration of a square to  $|0000\rangle$  or  $|1111\rangle$ , we can see that spins nearest to each square are indeed mapped to  $|0000\rangle + |1111\rangle$ .

Finally, we obtain a 2D toric code state on a square lattice with larger lattice constant. That is to say, after an ERG transformation composed of adding/removing product states and LU transformations, the structure of the 2D toric code ground state is preserved. Or from another perspective, the 2D toric code model is a fixed point of the ERG transformation symbolically denoted by Eq. (2). A pictorial demonstration of this ERG transformation is given in Fig. 3.

### B. Level-1 ERG transformation of $[0, 1, 2, 3]$ (3D X-cube) states

In this subsection, we review the ERG<sup>1</sup> transformation of the  $[0, 1, 2, 3]$  states following the recipe in Ref. [22]. Again, we firstly give an intuitive picture of the  $[0, 1, 2, 3]$  states based on the general discussion in Sec. II. In  $[0, 1, 2, 3]$  (a.k.a. X-cube) model, spins are located at links of a 3D cubic lattice. In this case,  $3 B_j^l$  terms with perpendicular  $l$ , where  $l$  denotes a plane containing vertex  $j$ , require  $j$  can only emanate 3 perpendicular strings composed of flipped spins (see Fig. 4 (a)), thus flipped spins must form ‘‘cages’’[36] in a superpositioned configuration. An  $A_i$  term flips the 12 spins on the links of cube  $i$ ,

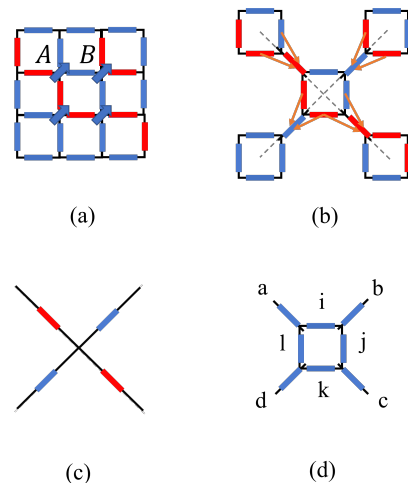


FIG. 3. **ERG transformation of the 2D toric code model labeled by  $[0, 1, 2, 2]$ .** This ERG transformation is denoted as ERG<sup>0</sup> in Eq. (2). In (a), we demonstrate how the original vertices are separated into two sublattices. A closed string configuration is illustrated, where  $|0\rangle$  spins on the links are denoted by blue bars, and  $|1\rangle$  spins forming strings are highlighted with red. The four blue arrows on four vertices denote four additional spins in state  $|0\rangle$ . In (b), we can see the four vertices are now extended to four links connecting plaquettes, and their corresponding additional spins, which are also denoted by bars now, *have been* transformed by CNOT gates such that the strings (formed by  $|1\rangle$  spins) are still closed. These CNOT gates targeting on the four additional spins are denoted by orange arrows pointing from control qubits to target qubits. Besides, dashed lines connecting the centers of squares are presented. As we can see, the action of CNOT gates couples additional and original spins in a manner that indeed preserves the closed strings pattern of 2D toric code ground state. By dropping all spins nearest to squares after another LU transformation, we obtain (c) in which a square lattice with a larger lattice constant appear and spins are located at the centers of new links (i.e., the dashed lines in (b)). We can see that, now spins on the centers of new links form a 2D toric code ground state on a new square lattice. In (d) we demonstrate an assignment of labels to the eight links around a square, where diagonal links are denoted by  $a, b, c$  and  $d$ , links nearest to the square are denoted by  $i, j, k$  and  $l$ .

thus contractible cages can freely fluctuate. We will see that, the ERG transformation indeed preserves this cage-net pattern of  $[0, 1, 2, 3]$  states.

We start with a ground state  $|\xi_i\rangle$  of the X-cube model defined on a cubic lattice of the size  $L_x \times L_y \times L_z$  with periodic boundary condition (PBC), and obtain a ground state  $|\xi_f\rangle$  on a cubic lattice of the size  $L_x \times L_y \times (L_z + 1)$  with PBC by the following transformations:

First, we choose a  $T^2$  (2-torus) composed by the centers of parallel links along direction  $\hat{z}$  with the same  $\hat{z}$ -coordinate, and regard the  $T^2$  as a cut: all links intersecting with the  $T^2$  are cut into 2 links. Without loss of generality, we assume the  $T^2$  is located at  $z = \frac{1}{2}$ , which means the cut links are of the form  $(i, j, \frac{1}{2})$ , where  $i, j$  are integers. After that, we apply a rescaling. For each cut link  $l = (i, j, \frac{1}{2})$ , we double the length of  $l$  to 2. Then, we can see that  $l$  is cut into links  $l_1 = (i, j, \frac{1}{2})$  and  $l_2 = (i, j, \frac{3}{2})$  of length 1, and now the cut  $T^2$  is located at

$z = 1$ . We assign the original spin on  $l$  to  $l_1$ .

Second, for each  $l_2$ , we put an additional spin of the state  $|0\rangle$  on it. It means that we enlarge the Hilbert space by taking a tensor product of the original one with the added spins, and add a series of  $-\sigma_{l_2}^z$  terms to the Hamiltonian to make all the added spins in the state  $|0\rangle$  (since a term  $-\sigma_{l_2}^z$  requires a ground state  $|\phi\rangle$  to satisfy  $\sigma_{l_2}^z|\phi\rangle = |\phi\rangle$ ). Then, for each original cut link  $l$ , we apply a CNOT gate with the original qubit on  $l_1$  as control qubit and the added one on  $l_2$  as target. By conjugate action of CNOT gates, the added  $-\sigma_{l_2}^z$  terms are mapped to  $-\sigma_{l_1}^z\sigma_{l_2}^z$  terms (see Appendix A). As a result, given a cut link  $l$ , for an arbitrary Ising configuration  $|\dots\sigma_l\dots\rangle$  from  $|\xi_i\rangle$  ( $\sigma_l = 0$  or  $1$ ), we have  $|\dots\sigma_l\dots\rangle \rightarrow |\dots\sigma_{l_1}\sigma_{l_2}\dots\rangle$ , where  $\sigma_{l_1} = \sigma_{l_2} = \sigma_l$  (see Fig. 4 (b)). The ground state transformed by steps above is denoted as  $|\xi_1\rangle$ .

Third, we insert a 2D toric code  $([0, 1, 2, 2])$  ground state  $|\xi_{gs}\rangle$  of the size  $L_x \times L_y$  on the cut  $T^2$  given in the first step. That is to say, the spins composing the inserted state are located on links of the form  $(i + \frac{1}{2}, j, 1)$  and  $(i, j + \frac{1}{2}, 1)$  in the rescaled lattice (see Fig. 4 (c), note that there are no spins on such links before this step). Then, we denote the tensor product of  $|\xi_1\rangle$  and  $|\xi_{gs}\rangle$  as  $|\xi_2\rangle = |\xi_1\rangle \otimes |\xi_{gs}\rangle$ . As 2D toric code model on a  $T^2$  is 4-fold degenerated, this step has 4 possible outcomes corresponding to 4 possible inserted 2D toric code ground states.

Finally, we act a series of CNOT gates on  $|\xi_2\rangle$  as illustrated in Fig. 4 (d). The CNOT gates are organized in a translational invariant manner, thus we only need to specify them for a specific cube. Without loss of generality, we take  $\gamma_3 = (\frac{1}{2}, \frac{1}{2}, \frac{1}{2})$ , and denote the vertices of  $\gamma_3$  by letters as shown in Fig. 4 (d). For example, we have  $e = (0, 0, 0)$  and  $c = (1, 1, 1)$ . Then, the CNOT gates can be explicitly specified as follows:

$$\begin{aligned}\sigma_{bc} &\rightarrow \sigma_{bf}, \sigma_{cg}, \sigma_{fg}; \\ \sigma_{ad} &\rightarrow \sigma_{ae}, \sigma_{dh}, \sigma_{eh}; \\ \sigma_{ab} &\rightarrow \sigma_{ef}; \\ \sigma_{dc} &\rightarrow \sigma_{hg};\end{aligned}$$

where  $\sigma_{xy}$  refers to the spin located on the link between  $x$  and  $y$  vertices,  $\rightarrow$  points from the control qubit to target qubits. Intuitively, we can see that by conjugate action (see Appendix A), the CNOT gates map the  $A_p = \sigma_{ab}^x \sigma_{bc}^x \sigma_{cd}^x \sigma_{da}^x$  stabilizer of the inserted 2D toric code ground state to  $A_c = \sigma_{ab}^x \sigma_{bc}^x \sigma_{cd}^x \sigma_{da}^x \sigma_{ef}^x \sigma_{fg}^x \sigma_{gh}^x \sigma_{he}^x \sigma_{ae}^x \sigma_{bf}^x \sigma_{cg}^x \sigma_{dh}^x$ , that is a stabilizer of X-cube ground state. Similarly, we can check that the CNOT gates generate all stabilizer generators we need to obtain X-cube ground states on a lattice of the size  $L_x \times L_y \times (L_z + 1)$  with PBC (see Sec. IV B for a more detailed demonstration).

Therefore, after the application of the CNOT gates, we obtain  $|\xi_f\rangle$ , which is a ground state of X-cube model on a lattice of the size  $L_x \times L_y \times (L_z + 1)$  with PBC. Pictorially, we can see the transformed state preserves the cage-net pattern of X-cube ground states.

Due to the fact that there are 4 possible choices of  $|\xi_{gs}\rangle$  in the third step, for a given  $|\xi_i\rangle$ , we have 4 possible  $|\xi_f\rangle$  outcomes. As a result, if we require the GSD formula to be symmetric for  $L_x$ ,  $L_y$  and  $L_z$ , the GSD of X-cube model has to satisfy  $\log_2 GSD = 2L_x + 2L_y + 2L_z + C$ , where  $C$

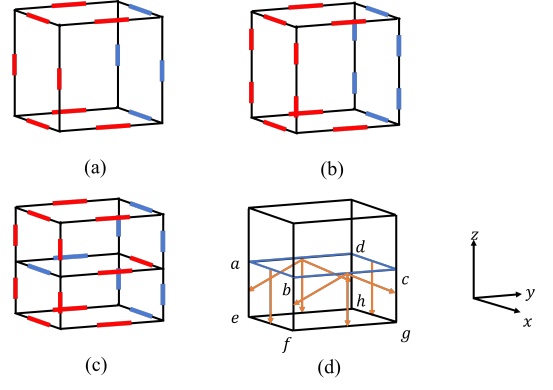


FIG. 4. **ERG transformation of the 3D X-cube model labeled by  $[0, 1, 2, 3]$ .** This ERG transformation is denoted as  $ERG^1$  in Eq. (3). We use red bars to denote spins occupied by strings in a configuration, and blue bars for the unoccupied ones. In (a), we demonstrate a configuration around the cube  $\gamma_3 = (\frac{1}{2}, \frac{1}{2}, \frac{1}{2})$  in the original  $|\xi_i\rangle$  state. In (b), we demonstrate the configuration obtained by cutting links of the form  $(i, j, \frac{1}{2})$ , adding additional spins and applying a series of CNOT gates (i.e., a configuration from  $|\xi_1\rangle$ ). In (c), we demonstrate a configuration after further inserting a 2D toric code ground state  $|\xi_{gs}\rangle$  (i.e., a configuration from  $|\xi_2\rangle = |\xi_1\rangle \otimes |\xi_{gs}\rangle$ ). In (d), we demonstrate the CNOT gates applied on  $|\xi_2\rangle$ . Here, we use a different notation for clarity. The control qubits, i.e., spins from the inserted 2D toric code ground state on plane  $z = 1$  (in the rescaled lattice), are denoted by blue links, while other spins are denoted by black links. The orange arrows point from control qubits to corresponding target qubits. Some vertices are denoted by letters.

is a constant. This result is consistent with the exact result given in Ref. [31, 33]. Besides, based on this method to obtain the GSD, we can see that the coefficients of linear terms in  $\log_2 GSD$  are directly related to the topology of the 2D subsystems (dubbed as “leaves”) of X-cube model.

### C. Level-2 ERG transformation of $[0, 1, 2, 4]$ states

In this subsection, we demonstrate the  $ERG^2$  transformation of  $[0, 1, 2, 4]$  states. Similar to  $[0, 1, 2, 3]$  model, here we give an intuitive picture of  $[0, 1, 2, 4]$  states based on the general discussion in Sec. II. In  $[0, 1, 2, 4]$  model, spins are located at links of a 4D hypercubic lattice. In this case,  $6 B_j^l$  terms with perpendicular  $l$ , where  $l$  denotes a plane containing vertex  $j$ , require  $j$  can only emanate 4 perpendicular strings composed of flipped spins. An  $A_i$  term flips the 32 spins on the links of hypercube  $i$ . We will see that, the ERG transformation indeed preserves the pattern of  $[0, 1, 2, 4]$  states.

Again, we start with a ground state  $|\xi_i\rangle$  of the  $[0, 1, 2, 4]$  model defined on a lattice of the size  $L_1 \times L_2 \times L_3 \times L_4$  with PBC, and obtain a ground state  $|\xi_f\rangle$  on a lattice of the size  $L_1 \times L_2 \times L_3 \times (L_4 + 1)$  with PBC. The  $ERG^2$  transformation can be described as follows:

First, we choose a  $T^3$  (3-torus) composed of the centers of parallel links along direction  $\hat{x}_4$  with the same  $\hat{x}_4$ -coordinate, and regard the  $T^3$  as a cut: all links intersecting with the  $T^3$  are cut into 2 links. Without loss of generality, we assume the

$T^3$  is located at  $x_4 = \frac{1}{2}$ , which means the cut links are of the form  $(i, j, k, \frac{1}{2})$ , where  $i, j, k$  are integers. After that, we apply a rescaling. For each cut link  $l = (i, j, k, \frac{1}{2})$ , we double the length of  $l$  to 2. Then, we can see that  $l$  is cut into links  $l_1 = (i, j, k, \frac{1}{2})$  and  $l_2 = (i, j, k, \frac{3}{2})$  of length 1, and now the cut  $T^3$  is located at  $x_4 = 1$ . We assign the original spin on  $l$  to  $l_1$ .

Second, for each  $l_2$ , we put an additional spin of the state  $|0\rangle$  on it. It means that we enlarge the Hilbert space by taking a tensor product of the original one with the added spins, and add a series of  $-\sigma_{l_2}^z$  terms to the Hamiltonian to make all the added spins in the state  $|0\rangle$  (since a  $-\sigma_{l_2}^z$  term requires a ground state  $|\phi\rangle$  to satisfy  $\sigma_{l_2}^z|\phi\rangle = |\phi\rangle$ ). Then, for each original cut link  $l$ , we apply a CNOT gate with the original qubit on  $l_1$  as control qubit and the added one on  $l_2$  as target. By conjugate action of CNOT gates, the added  $-\sigma_{l_2}^z$  terms are mapped to  $-\sigma_{l_1}^z\sigma_{l_2}^z$  terms (see Appendix A). As a result, given a cut link  $l$ , for an arbitrary Ising configuration  $|\dots\sigma_l\dots\rangle$  from  $|\xi_i\rangle$  ( $\sigma_l = 0$  or 1), we have  $|\dots\sigma_l\dots\rangle \rightarrow |\dots\sigma_{l_1}\sigma_{l_2}\dots\rangle$ , where  $\sigma_{l_1} = \sigma_{l_2} = \sigma_l$ . The ground state transformed by the steps above is denoted as  $|\xi_1\rangle$ .

Third, we insert a 3D X-cube ( $[0, 1, 2, 3]$ ) ground state  $|\xi_{gs}\rangle$  of the size  $L_1 \times L_2 \times L_3$  on the cut  $T^3$  given in the first step. That is to say, the spins composing the inserted state are located on links of the form  $(i + \frac{1}{2}, j, k, 1)$ ,  $(i, j + \frac{1}{2}, k, 1)$  and  $(i, j, k + \frac{1}{2}, 1)$  in the rescaled lattice (note that there are no spins on such links before this step). Then, we denote the tensor product of  $|\xi_1\rangle$  and  $|\xi_{gs}\rangle$  as  $|\xi_2\rangle = |\xi_1\rangle \otimes |\xi_{gs}\rangle$ . As 3D X-cube model on the  $T^3$  satisfies  $\log_2 GSD = 2L_1 + 2L_2 + 2L_3 - 3$ , this step has  $2^{2L_1+2L_2+2L_3-3}$  possible outcomes corresponding to  $2^{2L_1+2L_2+2L_3-3}$  possible inserted 3D X-cube ground states.

Finally, we act a series of CNOT gates on  $|\xi_2\rangle$  as illustrated in Fig. 5. The CNOT gates are organized in a translational invariant manner, thus we only need to specify them for a specific 4-cube. Without loss of generality, we take  $\gamma_4 = (\frac{1}{2}, \frac{1}{2}, \frac{1}{2}, \frac{1}{2})$ , and denote the vertices of  $\gamma_4$  by letters as shown in Fig. 5. Then, the CNOT gates can be explicitly specified as follows:

$$\begin{aligned} \sigma_{fg} &\rightarrow \sigma_{fn}, \sigma_{no}, \sigma_{og}; \\ \sigma_{bc} &\rightarrow \sigma_{bj}, \sigma_{jk}, \sigma_{kc}; \\ \sigma_{ad} &\rightarrow \sigma_{ai}, \sigma_{il}, \sigma_{ld}; \\ \sigma_{eh} &\rightarrow \sigma_{em}, \sigma_{mp}, \sigma_{ph}; \\ \sigma_{ef} &\rightarrow \sigma_{mn}; \\ \sigma_{ab} &\rightarrow \sigma_{ij}; \\ \sigma_{dc} &\rightarrow \sigma_{lk}; \\ \sigma_{hg} &\rightarrow \sigma_{po}; \\ \sigma_{cg} &\rightarrow \sigma_{ko}; \\ \sigma_{bf} &\rightarrow \sigma_{jn}; \\ \sigma_{ae} &\rightarrow \sigma_{im}; \\ \sigma_{dh} &\rightarrow \sigma_{lp}; \end{aligned}$$

where  $\sigma_{xy}$  refers to the spin located on the link between  $x$  and  $y$  vertices,  $\rightarrow$  points from the control qubit to target qubits.

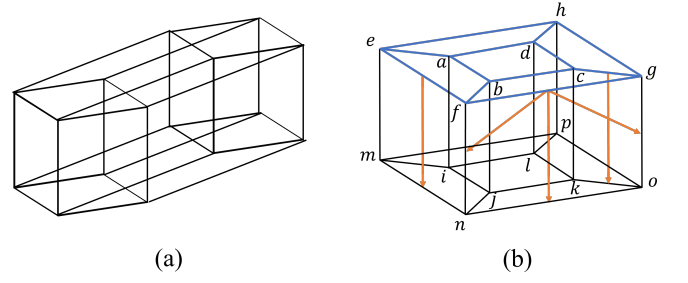


FIG. 5. **ERG transformation of the  $[0, 1, 2, 4]$  model.** Here we demonstrate the CNOT gates applied on  $|\xi_2\rangle$  following the same rules as in Fig. 4 (d). In (a), we give a schematic picture of a 4-cube, while in (b), we use another way to illustrate the 4-cube to show the CNOT gates more clearly. In (b), we use blue links to denote control qubits from the inserted X-cube ground state (a.k.a.  $[0, 1, 2, 3]$  state) on the cut  $T^3$  with  $x_4 = 1$ , and black links for the target qubits. For simplicity, orange arrows pointing from control qubits to target qubits are only presented for 3 control qubits along different directions. As we can see, these CNOT gates satisfy all conditions given in the general recipe in Sec. IV B.

Intuitively, we can see that by conjugate action (see Appendix A), the CNOT gates map the

$$A_c = \sigma_{ab}^x \sigma_{bc}^x \sigma_{cd}^x \sigma_{da}^x \sigma_{ae}^x \sigma_{bf}^x \sigma_{cg}^x \sigma_{dh}^x \sigma_{ef}^x \sigma_{fg}^x \sigma_{gh}^x \sigma_{he}^x,$$

stabilizer of the inserted 3D X-cube ground state to

$$\begin{aligned} A_{\gamma_4} &= \sigma_{ab}^x \sigma_{bc}^x \sigma_{cd}^x \sigma_{da}^x \sigma_{ae}^x \sigma_{bf}^x \sigma_{cg}^x \sigma_{dh}^x \\ &\quad \sigma_{ef}^x \sigma_{fg}^x \sigma_{gh}^x \sigma_{he}^x \sigma_{ij}^x \sigma_{jk}^x \sigma_{kl}^x \sigma_{li}^x \\ &\quad \sigma_{im}^x \sigma_{jn}^x \sigma_{ko}^x \sigma_{lp}^x \sigma_{mn}^x \sigma_{no}^x \sigma_{op}^x \sigma_{pm}^x \\ &\quad \sigma_{ai}^x \sigma_{bj}^x \sigma_{ck}^x \sigma_{dl}^x \sigma_{em}^x \sigma_{fn}^x \sigma_{go}^x \sigma_{hp}^x, \end{aligned}$$

that is a stabilizer of  $[0, 1, 2, 4]$  ground state. Similarly, we can check that the CNOT gates generate all stabilizer generators we need to obtain  $[0, 1, 2, 4]$  ground states on a lattice of the size  $L_1 \times L_2 \times L_3 \times (L_4 + 1)$  with PBC (see Sec. IV B for a more detailed demonstration). Therefore, after the application of the CNOT gates, we obtain  $|\xi_f\rangle$ , which is a ground state of  $[0, 1, 2, 4]$  model on a lattice of the size  $L_1 \times L_2 \times L_3 \times (L_4 + 1)$  with PBC.

Similar to X-cube model, we can see that the GSD of  $[0, 1, 2, 4]$  model has to satisfy  $\log_2 GSD = (2L_1 + 2L_2 + 2L_3 - 3)L_4 + C(L_1, L_2, L_3)$ , where  $C(L_1, L_2, L_3)$  is a function of  $L_1, L_2$  and  $L_3$ . When we require the GSD formula to be symmetric for  $L_1, L_2, L_3$  and  $L_4$ , then we have  $\log_2 GSD = 2L_1L_2 + 2L_1L_3 + 2L_1L_4 + 2L_2L_3 + 2L_2L_4 + 2L_3L_4 - 3L_1 - 3L_2 - 3L_3 - 3L_4 + C'$ , where  $C'$  is a constant. This result is consistent with the result obtained by ground state decomposition in Ref. [33].

#### D. Level-1 ERG transformation of $[1, 2, 3, 4]$ states

For comparison, in this subsection, we demonstrate the ERG<sup>1</sup> transformation of  $[1, 2, 3, 4]$  states. We will see that,

though  $[1, 2, 3, 4]$  model has the same spatial dimension as  $[0, 1, 2, 4]$  model, in the ERG transformation of its ground states we only need to add/remove LRE<sup>1</sup> rather than LRE<sup>2</sup> states. Before the demonstration, here we also give an intuitive picture of  $[1, 2, 3, 4]$  states based on the general discussion in Sec. II. In  $[1, 2, 3, 4]$  model, spins are located at plaquettes of a 4D hypercubic lattice. In this case,  $3 B_j^l$  terms with perpendicular  $l$ , where  $l$  denotes a 3D subsystem containing link  $j$ , require  $j$  can only emanate 3 perpendicular membranes composed of flipped spins. An  $A_i$  term flips the 24 spins on the plaquettes of hypercube  $i$ . We will see that, the ERG transformation indeed preserves the pattern of  $[1, 2, 3, 4]$  states.

Again, we start with a ground state  $|\xi_i\rangle$  of the  $[1, 2, 3, 4]$  model defined on a lattice of the size  $L_1 \times L_2 \times L_3 \times L_4$  with PBC, and obtain such a ground state  $|\xi_f\rangle$  on a lattice of the size  $L_1 \times L_2 \times L_3 \times (L_4 + 1)$  with PBC. The ERG<sup>1</sup> transformation can be similarly described as follows:

First, we choose a  $T^3$  (3-torus) composed of the centers of parallel links along direction  $\hat{x}_4$  with the same  $\hat{x}_4$ -coordinate, and regard the  $T^3$  as a cut: all plaquettes intersecting with the  $T^3$  are cut into 2 plaquettes. Without loss of generality, we assume the  $T^3$  is located at  $x_4 = \frac{1}{2}$ , which means the cut plaquettes are of the form  $(i, j, k, \frac{1}{2}) + \frac{1}{2}I_n$ , where  $n = 1, 2, 3$ ,  $I_n$  is the unit vector along  $\hat{x}_n$  direction,  $i, j, k$  are integers. After that, we apply a rescaling. For each cut plaquette  $p = (i, j, k, \frac{1}{2}) + \frac{1}{2}I_n$ , we double the linear size of  $p$  along  $\hat{x}_4$  direction to 2. Then, we can see that  $p$  is cut into plaquettes  $p_1 = (i, j, k, \frac{1}{2}) + \frac{1}{2}I_n$  and  $p_2 = (i, j, k, \frac{3}{2}) + \frac{1}{2}I_n$  with linear sizes along  $\hat{x}_4$  direction equal to 1, and now the cut  $T^3$  is located at  $x_4 = 1$ . We can assign the original spin on  $p$  to  $p_1$ .

Second, for each  $p_2$ , we put an additional spin of the state  $|0\rangle$  on it. Equivalently, it means that we enlarge the Hilbert space by taking a tensor product of the original one with the added spins, and add a series of  $-\sigma_{p_2}^z$  terms to the Hamiltonian to make all the added spins in the state  $|0\rangle$  (since a  $-\sigma_{p_2}^z$  term requires a ground state  $|\phi\rangle$  to satisfy  $\sigma_{p_2}^z|\phi\rangle = |\phi\rangle$ ). Then, for each original cut plaquette  $p$ , we apply a CNOT gate with the original qubit on  $p_1$  as control qubit and the added one on  $p_2$  as target. By conjugate action of CNOT gates, the added  $-\sigma_{p_2}^z$  terms are mapped to  $-\sigma_{p_1}^z \sigma_{p_2}^z$  terms (see Appendix A). As a result, given a cut plaquette  $p$ , for an arbitrary Ising configuration  $|\cdots \sigma_p \cdots\rangle$  from  $|\xi_i\rangle$  ( $\sigma_p = 0$  or 1), we have  $|\cdots \sigma_p \cdots\rangle \rightarrow |\cdots \sigma_{p_1} \sigma_{p_2} \cdots\rangle$ , where  $\sigma_{p_1} = \sigma_{p_2} = \sigma_p$ . The ground state transformed by the steps above is denoted as  $|\xi_1\rangle$ .

Third, we insert a 3D toric code ( $[1, 2, 3, 3]$ ) ground state  $|\xi_{gs}\rangle$  of the size  $L_1 \times L_2 \times L_3$  on the cut  $T^3$  given in the first step. That is to say, the spins composing the inserted state are located on plaquettes of the form  $(i + \frac{1}{2}, j + \frac{1}{2}, k, 1)$ ,  $(i, j + \frac{1}{2}, k + \frac{1}{2}, 1)$  and  $(i + \frac{1}{2}, j, k + \frac{1}{2}, 1)$  in the rescaled lattice (note that there are no spins on such plaquettes before this step). Then, we denote the tensor product of  $|\xi_1\rangle$  and  $|\xi_{gs}\rangle$  as  $|\xi_2\rangle = |\xi_1\rangle \otimes |\xi_{gs}\rangle$ . As 3D toric code model on the  $T^3$  satisfies  $\log_2 GSD = 3$ [35, 37], this step has  $2^3$  possible outcomes corresponding to  $2^3$  possible inserted 3D toric code ground states.

Finally, we act a series of CNOT gates on  $|\xi_2\rangle$  as illustrated in

Fig. 6. The CNOT gates are organized in a translational invariant manner, thus we only need to specify them for a specific 4-cube. Without loss of generality, we take  $\gamma_4 = (\frac{1}{2}, \frac{1}{2}, \frac{1}{2}, \frac{1}{2})$ , and denote the vertices of  $\gamma_4$  by letters as shown in Fig. 6. Then, the CNOT gates can be explicitly specified as follows:

$$\begin{aligned} \sigma_{abcd} &\rightarrow \sigma_{ijkl}, \sigma_{abji}, \sigma_{bckj}, \sigma_{cdlk}, \sigma_{dail}; \\ \sigma_{efgh} &\rightarrow \sigma_{mnop}, \sigma_{efnm}, \sigma_{fgon}, \sigma_{ghpo}, \sigma_{hemp}; \\ \sigma_{abfe} &\rightarrow \sigma_{ijnm}, \sigma_{aemi}, \sigma_{bfjn}; \\ \sigma_{cdhg} &\rightarrow \sigma_{klpo}, \sigma_{dhpl}, \sigma_{cgok}; \\ \sigma_{bcgf} &\rightarrow \sigma_{jkon}; \\ \sigma_{daeh} &\rightarrow \sigma_{limp}; \end{aligned}$$

where  $\sigma_{xyzw}$  refers to the spin located on the plaquette between  $x, y, z$  and  $w$  vertices,  $\rightarrow$  points from the control qubit to target qubits. Intuitively, we can see that by conjugate action (see Appendix A), the CNOT gates map the

$$A_c = \sigma_{abcd}^x \sigma_{efgh}^x \sigma_{abfe}^x \sigma_{bcgf}^x \sigma_{cdhg}^x \sigma_{daeh}^x,$$

stabilizer of the inserted 3D toric code ground state to

$$\begin{aligned} A_{\gamma_4} &= \sigma_{abcd}^x \sigma_{efgh}^x \sigma_{abfe}^x \sigma_{bcgf}^x \sigma_{cdhg}^x \sigma_{daeh}^x \\ &\quad \sigma_{ijkl}^x \sigma_{mnop}^x \sigma_{ijnm}^x \sigma_{jkon}^x \sigma_{klpo}^x \sigma_{limp}^x \\ &\quad \sigma_{aemi}^x \sigma_{bfjn}^x \sigma_{efnm}^x \sigma_{abji}^x \sigma_{bckj}^x \sigma_{fgon}^x \\ &\quad \sigma_{cgok}^x \sigma_{dhpl}^x \sigma_{ghpo}^x \sigma_{cdlk}^x \sigma_{dail}^x \sigma_{hemp}^x, \end{aligned}$$

that is a stabilizer of  $[1, 2, 3, 4]$  ground state. Similarly, we can check that the CNOT gates generate all stabilizer generators we need to obtain  $[1, 2, 3, 4]$  ground states on a lattice of the size  $L_1 \times L_2 \times L_3 \times (L_4 + 1)$  with PBC (see Sec. IV B for a more detailed demonstration). Therefore, after the application of the CNOT gates, we obtain  $|\xi_f\rangle$ , which is a ground state of  $[1, 2, 3, 4]$  model on a lattice of the size  $L_1 \times L_2 \times L_3 \times (L_4 + 1)$  with PBC.

Similar to X-cube model, we can see that the GSD of  $[1, 2, 3, 4]$  model has to satisfy  $\log_2 GSD = 3 \times L_4 + C(L_1, L_2, L_3)$ , where  $C(L_1, L_2, L_3)$  is a function of  $L_1, L_2$  and  $L_3$ . When we require the GSD formula to be symmetric for  $L_1, L_2, L_3$  and  $L_4$ , then we have  $\log_2 GSD = 3L_1 + 3L_2 + 3L_3 + 3L_4 + C'$ , where  $C'$  is a constant. This result is consistent with the result obtained by ground state decomposition in Ref. [33].

#### IV. ENTANGLEMENT RENORMALIZATION GROUP OF GENERIC LEVELS

In this section, we firstly show a generic recipe of the construction of ERG <sup>$D-d-2$</sup>  transformations of  $[d, d+1, d+2, D]$  models with  $D > d+2$ . After that, in Sec. IV B, we prove that for such  $[d, d+1, d+2, D]$  models, the constructed ERG transformations indeed give ground states of the same model of different sizes, i.e., the models are fixed points of the corresponding ERG transformations. Finally, in Sec. IV C, we discuss about the hierarchy of ERG transformations and LRE



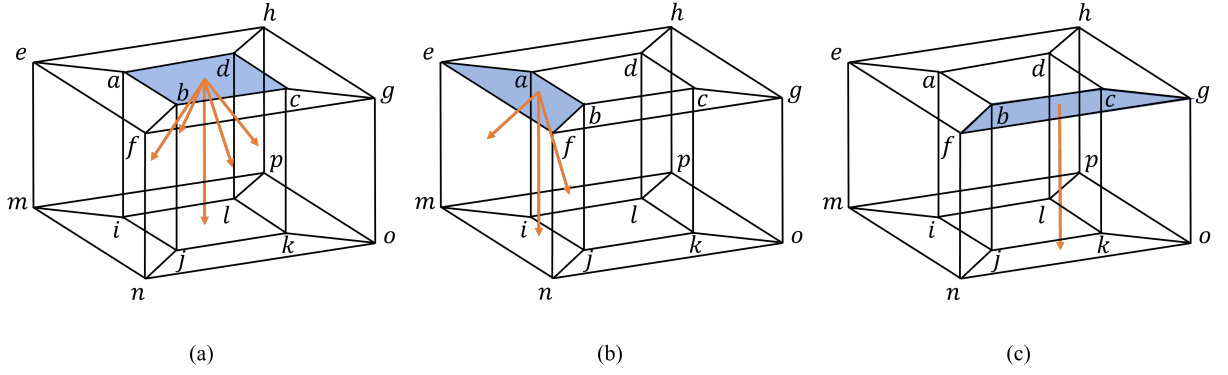


FIG. 6. **ERG transformation of the  $[1, 2, 3, 4]$  model.** Here we follow a similar notation as in Fig. 5 (b) to demonstrate the CNOT gates applied on  $|\xi_2\rangle$ . Again, we set qubits nearest to the cube specified by  $abcdefgh$  as from the inserted 3D toric code ground state (a.k.a.  $[1, 2, 3, 3]$  state) on the cut  $T^3$  with  $x_4 = 1$ . For clarity, here we only demonstrate 3 control qubits and their associated CNOT gates. In (a), (b) and (c), we use three transparent plaquettes highlighted with blue to denote three different control qubits, and present orange arrows pointing from control qubits to target ones. Here it should be noticed that two different plaquettes may share the same center in these pictures, like  $abcd$  and  $efgh$ . As we can see, these CNOT gates satisfy all conditions given in the general recipe in Sec. IV B.

states based on the constructed ERG transformations. Note that  $\text{ERG}^0$  transformations of  $[D-2, D-1, D, D]$  models are not included in this recipe.

#### A. Level- $(D-d-2)$ ERG transformation of $[d, d+1, d+2, D]$ states

In general, for a  $[d, d+1, d+2, D]$  model with  $D > d+2$ , we can demonstrate the  $\text{ERG}^{D-d-2}$  transformation of  $[d, d+1, d+2, D]$  states. Again, we start with a ground state  $|\xi_i\rangle$  of  $[d, d+1, d+2, D]$  model defined on a lattice of the size  $L_1 \times L_2 \times \cdots \times L_D$  with PBC, and obtain a ground state  $|\xi_f\rangle$  on a lattice of the size  $L_1 \times L_2 \times \cdots \times (L_D + 1)$  with PBC. The  $\text{ERG}^{D-d-2}$  transformation can be described as follows:

1. First, we choose a  $(D-1)$ -torus  $T^{D-1}$  composed of the centers of links with the same  $\hat{x}_D$ -coordinate. Without loss of generality, we set the chosen  $T^{D-1}$  to be located at  $x_D = \frac{1}{2}$ , such that it is composed of the centers of links of the form  $(n_1, n_2, \dots, n_{D-1}, \frac{1}{2})$ , where  $n_1, n_2, \dots, n_{D-1}$  are integers. Then we regard the  $T^{D-1}$  as a cut: every  $\gamma_{d+1}$  intersecting with the  $T^{D-1}$  is cut into 2  $\gamma_{d+1}$ 's with identical spins. That is to say, for each cut  $\gamma_{d+1}$ , we put an additional spin in the state  $|0\rangle$ , and then apply a CNOT gate with the original qubit as control qubit and the added one as target. In consequence, given a cut  $\gamma_{d+1}$ , for an arbitrary Ising configuration  $|\cdots \sigma_{\gamma_{d+1}} \cdots\rangle$  from  $|\xi_i\rangle$  ( $\sigma_{\gamma_{d+1}} = 0$  or 1), we have  $|\cdots \sigma_{\gamma_{d+1}} \cdots\rangle \rightarrow |\cdots \sigma_{(\gamma_{d+1})_1} \sigma_{(\gamma_{d+1})_2} \cdots\rangle$ , where  $\sigma_{(\gamma_{d+1})_1} = \sigma_{(\gamma_{d+1})_2} = \sigma_{\gamma_{d+1}}$ . Then, we rescale the lattice by extending the linear size of the cut  $\gamma_{d+1}$  along  $\hat{x}_D$  direction to 2, such that now the chosen  $T^{D-1}$  is composed of sites of the form  $(n_1, n_2, \dots, n_{D-1}, 1)$ , and for a cut  $\gamma_{d+1} = (\cdots, \frac{1}{2})$  in the original lattice, the original and additional spins are respectively assigned to  $(\gamma_{d+1})_1 = (\cdots, \frac{1}{2})$  and  $(\gamma_{d+1})_2 = (\cdots, \frac{3}{2})$  in the

rescaled lattice. The ground state transformed by this step is denoted as  $|\xi_1\rangle$ .

2. Second, we put a  $[d, d+1, d+2, D-1]$  ground state  $|\xi_{gs}\rangle$  of the size  $L_1 \times \cdots \times L_{D-1}$  on the  $T^{D-1}$  given in the previous step. That is to say, we can regard the  $(n_1, n_2, \dots, n_{D-1}, 1)$  sites as forming a hypercubic lattice defined on the  $T^{D-1}$ , and consider a  $[d, d+1, d+2, D-1]$  ground state  $|\xi_{gs}\rangle$  defined on this lattice. Then, by taking the tensor product of  $|\xi_1\rangle$  and  $|\xi_{gs}\rangle$ , we obtain  $|\xi_2\rangle = |\xi_1\rangle \otimes |\xi_{gs}\rangle$ .
3. Third, we act an LU transformation  $\mathcal{U}$  composed of a series of CNOT gates on  $|\xi_2\rangle$  (see Sec. IV B for a demonstration of this LU transformation  $\mathcal{U}$ ). After that, we obtain  $|\xi_f\rangle$ , which is a ground state of  $[d, d+1, d+2, D]$  model on a lattice of the size  $L_1 \times L_2 \times \cdots \times (L_D + 1)$  with PBC.

To see that the results are consistent with the results obtained by ground state decomposition in Ref. [33], without loss of generality, say that in the polynomial  $\log_2 \text{GSD}$  of  $[d, d+1, d+2, D-1]$  model on the  $T^{D-1}$ , the coefficient of  $L_i L_j \cdots L_n$  term is  $c$  (here  $i < j < \cdots < n < D$  is assumed). Then, the above ERG transformation requires that the number of copies of  $c L_i L_j \cdots L_n$  contained in the  $\log_2 \text{GSD}$  of  $[d, d+1, d+2, D]$  model grows linearly with  $L_D$ . That is to say, the polynomial  $\log_2 \text{GSD}$  of the  $[d, d+1, d+2, D]$  model has to contain the term  $c L_i L_j \cdots L_n L_D$ . This result is consistent with the relevant results from Ref. [33].

#### B. $[d, d+1, d+2, D]$ models as fixed points of level- $(D-d-2)$ ERG transformations

In this subsection, we give the conditions that an LU transformation  $\mathcal{U}$  used in the Step 3 of the  $\text{ERG}^{D-d-2}$  transformation of a general  $[d, d+1, d+2, D]$  state should satisfy,

and prove that the such an LU transformation  $\mathcal{U}$  indeed gives ground states of the  $[d, d+1, d+2, D]$  model on a lattice of different sizes, by considering the conjugate action of  $\mathcal{U}$  on the Hamiltonian terms. Without loss of generality, we assume the cut  $T^{D-1}$  is extended along  $\hat{x}_1, \hat{x}_2, \dots, \hat{x}_{D-1}$  directions, and the location is given by  $x_D = 1$  (in the rescaled lattice). For convenience, here we explicitly write down the Hamiltonian of a  $[d, d+1, d+2, D]$  model as below:

$$H_{[d, d+1, d+2, D]} = - \sum_{\gamma_D} A_{\gamma_D} - \sum_{\gamma_d} \sum_l B_{\gamma_d}^l, \quad (7)$$

where an  $A_{\gamma_D}$  term is the product of the  $x$ -components of the  $\binom{D}{d+1} \cdot 2^{D-d-1}$  spins nearest to the  $\gamma_D$ , a  $B_{\gamma_d}^l$  term is the product of the  $z$ -components of the 4 spins that (a) nearest to the  $\gamma_d$  and (b) living in the  $(d+2)$ -dimensional subsystem  $l$ .

We start with the conditions that the LU transformation  $\mathcal{U}$  should satisfy. According to the LU transformation  $\mathcal{U}$  of  $[0, 1, 2, 3]$ ,  $[0, 1, 2, 4]$  and  $[1, 2, 3, 4]$  models (i.e., the CNOT gates applied on  $|\xi_2\rangle$  states of corresponding subsections), we expect such an LU transformation in the  $\text{ERG}^{D-d-2}$  transformation of a general  $[d, d+1, d+2, D]$  state to satisfy the following conditions:

- First, we require  $\mathcal{U}$  to be composed of a series of CNOT gates around  $\gamma_D$ 's with  $x_D = \frac{1}{2}$ , where all control qubits are from the cut  $T^{D-1}$  (i.e., being located on  $\gamma_{d+1}$ 's with  $x_D = 1$ ). Besides, we require  $\mathcal{U}$  to be translational invariant, such that the application of the CNOT gates is the same for every applied  $\gamma_D$ . Therefore, we only need to consider the application of CNOT gates in a single  $\gamma_D$  to specify  $\mathcal{U}$ . Without loss of generality, we can focus on  $\gamma_D^r = (\frac{1}{2}, \frac{1}{2}, \dots, \frac{1}{2})$ . Here the superscript  $r$  is for reference.
- Second, for each  $\gamma_{d+1}$  in  $\gamma_D^r$  with  $x_D = 0$ , we require the qubit on it to be controlled by the qubit on  $\gamma_{d+1} + I_D$ , where  $I_D = (0, 0, \dots, 0, 1)$  is the unit vector along  $\hat{x}_D$  direction. Obviously, the qubit on such a  $\gamma_{d+1}$  is only controlled by 1 control qubit in  $\gamma_D^r$ .
- Third, for each  $\gamma_{d+1}$  in  $\gamma_D^r$  with  $x_D = \frac{1}{2}$ , we require the qubit on it to be controlled by exactly 1 nearest control qubit in  $\gamma_D^r$ . Besides, for a pair of nearest parallel qubits, we require them to be simultaneously controlled (or not) by the control qubit that links them. For example, a pair of nearest parallel qubits respectively defined on  $(\underbrace{\frac{1}{2}, \frac{1}{2}, \dots, \frac{1}{2}}_d, \underbrace{0, 0, \dots, 0}_{D-d}, \frac{1}{2})$  and

$$\left( \underbrace{\frac{1}{2}, \frac{1}{2}, \dots, \frac{1}{2}}_d, \underbrace{1, 0, \dots, 0}_{D-d}, \frac{1}{2} \right)$$

are either both controlled by  $(\underbrace{\frac{1}{2}, \frac{1}{2}, \dots, \frac{1}{2}}_d, \underbrace{\frac{1}{2}, \frac{1}{2}, \dots, \frac{1}{2}}_{D-d}, 0, \dots, 0, 1)$  or not (here we can

notice that this control qubit is the only one that links the pair, i.e., simultaneously being nearest to the pair of qubits).

The existence of such LU transformations is obvious. And we can check that when  $d = 0, D = 3$ ,  $d = 0, D = 4$  and  $d = 1, D = 4$ , the LU transformations  $\mathcal{U}$  in the ERG transformations of  $[0, 1, 2, 3]$ ,  $[0, 1, 2, 4]$  and  $[1, 2, 3, 4]$  states all satisfy the above conditions. Besides, here we should notice that each target qubit  $\sigma_i$  with  $x_D = \frac{1}{2}$  is always controlled by two qubits. Without loss of generality, say the qubit  $\sigma_i$  on  $(d+1)$ -cube  $i = (\underbrace{\frac{1}{2}, \frac{1}{2}, \dots, \frac{1}{2}}_d, \underbrace{0, 0, \dots, 0}_{D-d}, \frac{1}{2})$  is controlled

by the qubit on  $i_c = (\underbrace{\frac{1}{2}, \frac{1}{2}, \dots, \frac{1}{2}}_d, \underbrace{\frac{1}{2}, \frac{1}{2}, \dots, \frac{1}{2}}_{D-d}, 0, \dots, 0, 1)$ , accord-

ing to the translational invariance of the LU transformation, the qubit on  $i' = i - I_{d+1} = (\underbrace{\frac{1}{2}, \frac{1}{2}, \dots, \frac{1}{2}}_d, \underbrace{-1, 0, \dots, 0}_{D-d}, \frac{1}{2})$

must be controlled by the qubit on  $i'_c = i_c - I_{d+1} = (\underbrace{\frac{1}{2}, \frac{1}{2}, \dots, \frac{1}{2}}_d, \underbrace{-\frac{1}{2}, 0, \dots, 0}_{D-d}, 1)$ ; after that, as  $i$  and  $i'$  are

parallel  $(d+1)$ -cubes connected by  $i'_c$ ,  $\sigma_i$  must also be controlled by the qubit on  $i'_c$ . Then, we can notice that an arbitrary  $\gamma_D$  nearest to  $i$  has the form  $(\underbrace{\frac{1}{2}, \frac{1}{2}, \dots, \frac{1}{2}}_d, \underbrace{\pm \frac{1}{2}, \pm \frac{1}{2}, \dots, \pm \frac{1}{2}}_{D-d}, \frac{1}{2})$ , thus it must be either

nearest to  $i_c$  or  $i'_c$ . Since a target qubit can only be controlled by 1 control qubit from a nearest  $\gamma_D$  as required by the conditions above, no other qubits in the  $T^{D-1}$  can control  $\sigma_i$ . In conclusion, for any target qubit  $\sigma_i$  with  $x_D = \frac{1}{2}$ , there are always 2 qubits that control it.

Then, we show that though the concrete form of the LU transformation  $\mathcal{U}$  has not been specified, the above conditions can make sure that  $\mathcal{U}$  produces the ground states as expected. That is to say, for an LU transformation  $\mathcal{U}$  satisfying the conditions above, a  $|\xi_f\rangle = \mathcal{U}|\xi_2\rangle$  is indeed a ground state of  $[d, d+1, d+2, D]$  model.

At first, we notice that  $\mathcal{U}$  is applied on the  $|\xi_2\rangle$  given in Sec. IV A, and  $|\xi_2\rangle$  can be obtained as a ground state of the following Hamiltonian:

$$H_1 = H_{dddD} + H_{dddD-1} + H_{zz}, \quad (8)$$

where  $H_{dddD}$  refers to the terms in the original  $[d, d+1, d+2, D]$  model with some modifications according to the cut  $\gamma_{d+1}$ 's (see below),  $H_{dddD-1}$  refers to the terms of the  $[d, d+1, d+2, D-1]$  Hamiltonian on the cut  $T^{D-1}$ , and  $H_{zz} = -\sum_i \sigma_i^z \sigma_{i+I_D}^z$  is added to make each pair of spins on a cut  $\gamma_{d+1}$  identical, where  $i$  refers to a  $(d+1)$ -cube with  $x_D = \frac{1}{2}$  in the rescaled lattice. Note that the  $A_{\gamma_D}$  terms in  $H_{dddD}$  near the  $T^{D-1}$  are modified to  $A'_{\gamma_D} = A_{\gamma_D} A_{\gamma_D+I_D}$  to be consistent with the cut  $\gamma_{d+1}$ 's, where  $A_{\gamma_D}$  and  $A_{\gamma_D+I_D}$  have the same form as an ordinary  $A$  term from the original  $[d, d+1, d+2, D]$  model, and  $\gamma_D$  satisfies  $x_D = \frac{1}{2}$ . As a concrete example, in  $[0, 1, 2, 4]$  model, where  $d = 0$ ,  $D = 4$ , such a modified  $A_{\gamma_4}$ , denoted as  $A'_{\gamma_4}$ , is given by  $A'_{\frac{1}{2}, \frac{1}{2}, \frac{1}{2}, \frac{1}{2}} = A_{\frac{1}{2}, \frac{1}{2}, \frac{1}{2}, \frac{1}{2}} A_{\frac{1}{2}, \frac{1}{2}, \frac{1}{2}, \frac{3}{2}}$ , where operators  $A_{\frac{1}{2}, \frac{1}{2}, \frac{1}{2}, \frac{1}{2}}$

and  $A_{\frac{1}{2}, \frac{1}{2}, \frac{1}{2}, \frac{3}{2}}$  themselves do not present in  $H_{dddD}$ . Furthermore, for a  $B_{\gamma_d}$  term from  $H_{dddD}$  with  $x_D = 2$  that involves qubit  $\sigma_i$  with  $x_D = \frac{1}{2}$ , we can replace it by the product of the  $B$  term itself and a corresponding  $\sigma_i^z \sigma_{i+I_D}^z$  term, such that the  $\sigma_i^z$  in the  $B$  term is replaced by  $\sigma_{i+I_D}^z$ . This modification makes such  $B$  terms “connected”. For example, in  $[0, 1, 2, 3]$  model, due to our assignment that for a cut link the original qubit is put on a link of the form  $(\dots, \frac{1}{2})$ , in the rescaled lattice, we would have  $B$  terms such as  $B_{(0,0,2)}^x = \sigma_{(0, \frac{1}{2}, 2)}^z \sigma_{(0, -\frac{1}{2}, 2)}^z \sigma_{(0,0, \frac{5}{2})}^z \sigma_{(0,0, \frac{1}{2})}^z$ , that is not connected, without such modifications. Similarly, we can freely add  $B_{\gamma_d}$  terms with  $x_D = \frac{3}{2}$  to  $H_1$  as such terms can be directly obtained by taking the products of  $B_{\gamma_d}$  terms with  $x_D = \frac{1}{2}$  and corresponding  $\sigma_i^z \sigma_{i+I_D}^z$  terms. Besides,  $H_{dddD}$  contains no  $B_{\gamma_d}$  terms on the  $T^{D-1}$ . After that, we can see that all terms in  $H_1$  still commute with each other. From another perspective,  $H_1$  can also be obtained by considering the conjugate action of the CNOT gates applied in the first step in Sec. IV A. A more detailed demonstration of the terms in  $H_1$  is given in Appendix B.

Secondly, because the  $\mathcal{U}$  transformation is a product of a series of CNOT gates, then, a transformed ground state  $\mathcal{U}|\phi\rangle$  satisfies  $(\mathcal{U}G\mathcal{U}^\dagger)\mathcal{U}|\phi\rangle = \mathcal{U}|\phi\rangle$ , where  $G$  is an arbitrary stabilizer from  $H_1$ . That is to say,  $\mathcal{U}|\phi\rangle$  is a ground state of the transformed Hamiltonian  $H_2$ , and  $H_2$  is composed of transformed stabilizers  $G' \equiv \mathcal{U}G\mathcal{U}^\dagger$ .

After that, we notice that the conjugate action of  $\mathcal{U}$  on a stabilizer  $G$  can be reduced to the conjugate action of CNOT gates on  $G$ . With the general mapping rules given by the conjugate action of CNOT gates (see Appendix A), we can obtain all terms in  $H_2$  as follows:

1. First, since for an arbitrary  $\gamma_{D-1}$  inside the  $T^{D-1}$ , all qubits that are controlled by the qubits from the  $\gamma_{D-1}$  together with the control qubits themselves form a  $\gamma_D$  with  $x_D = \frac{1}{2}$ ,  $A_{\gamma_{D-1}}$  terms in  $H_{dddD-1}$  are mapped to  $A_{\gamma_D}$  terms with  $x_D = \frac{1}{2}$ .
2. Second, since an arbitrary target qubit  $\sigma_i$  with  $x_D = \frac{1}{2}$  is controlled by exactly 2 qubits from the  $T^{D-1}$ , each  $\sigma_i^z \sigma_{i+I_D}^z$  term in  $H_{zz}$  is mapped to a 4-spin term composed of the original  $\sigma_i^z$ ,  $\sigma_{i+I_D}^z$  and the  $z$  components of the 2 qubits that control  $\sigma_i$ .
3. Third, further considering that an arbitrary target qubit  $\sigma_i$  with  $x_D = 0$  is only controlled by  $\sigma_{i+I_D}$  from the  $T^{D-1}$ , a  $B_{\gamma_d}$  term in  $H_{dddD}$  near the  $T^{D-1}$  should be modified as follows: (a) for a qubit  $\sigma_i$  with  $x_D = 0$  involved in the  $B$  term, multiply the term by  $\sigma_{i+I_D}^z$ ; (b) for a qubit  $\sigma_i$  with  $x_D = \frac{1}{2}$  involved in the  $B$  term, multiply the term by the  $z$  components of the 2 qubits that control the  $\sigma_i$ . As an example, for a  $B_{\gamma_d}$  term only involving qubits with  $x_D = 0$ , it is mapped to a  $B_{\gamma_d} B_{\gamma_d+I_D}$  term, where  $B_{\gamma_d+I_D}$  is obtained by adding  $I_D$  to the coordinates of all qubits involved in  $B_{\gamma_d}$ .
4. Finally, all other terms stay invariant under the conjugate action of  $\mathcal{U}$ .

We denote the Hamiltonian of  $[d, d+1, d+2, D]$  model on the lattice of the size  $L_1 \times L_2 \times \dots \times (L_D + 1)$  with PBC as  $H_3$  (see Eq. 7). Then we can notice that by taking the product of  $A$  terms obtained in the first step and  $A'$  terms from  $H_{dddD}$  we can obtain all  $A$  terms that exist in  $H_3$  but superficially missing in  $H_2$ ; by taking the product of the 4-spin terms obtained in the second step (which can be recognized as  $B$  terms in  $H_3$ ), modified  $B$  terms obtained in the third step and  $B$  terms in  $H_{dddD-1}$  we can obtain all  $B$  terms that exist in  $H_3$  but superficially missing in  $H_2$ . Therefore, all terms of  $H_3$  can be obtained by taking the product of terms of  $H_2$  (a more detailed demonstration is given in Appendix B). As it is also straightforward to check the other way around, finally, we can see that  $H_2$  and  $H_3$  are equivalent Pauli stabilizer code models with equivalent stabilizer groups, and  $|\xi_f\rangle = \mathcal{U}|\xi_2\rangle$  is indeed a ground state of  $H_3$ .

### C. Discussion

As we have demonstrated in this section, in the ERG transformations of different  $[d, d+1, d+2, D]$  states, the added/removed states are also different LRE states. From another word, the entanglement patterns in  $[d, d+1, d+2, D]$  states with different  $D$  and a fixed  $d$  are intrinsically different, and these models cannot be fully understood as fixed points of a finite number of types of ERG transformations. Instead, we need a infinite series of ERG transformations of different levels to understand the more general long range entanglement patterns.

Therefore, we conclude the above observations by proposing the definition of a hierarchy of ERG transformations, where each transformation is assigned with an integer level. Correspondingly, LRE states are assigned with integer levels as well (see Fig. 1). For a given stabilizer code model considered in this paper, two level- $(n+1)$  LRE ( $\text{LRE}^{n+1}$ ) states of different sizes can be connected by a level- $n$  ERG ( $\text{ERG}^n$ ) transformation, that is composed of LU transformations combined with addition/removal of level- $n$  LRE states. By this definition, if we define product states and short range entangled states as  $\text{LRE}^0$  states, then we have 2D toric code ( $[0, 1, 2, 2]$ ) states as  $\text{LRE}^1$  states, 3D X-cube ( $[0, 1, 2, 3]$ ) states as  $\text{LRE}^2$  states,  $[0, 1, 2, 4]$  states as  $\text{LRE}^3$  states and so on. Then, we can see that low level LRE states themselves can be recognized as trivial high level LRE states, just like a product state is recognized as a trivial pure topological order. Besides, a decoupled stack of  $\text{LRE}^n$  states is also a trivial  $\text{LRE}^{n+1}$  state, as it can reduced to nothing under a  $\text{ERG}^n$  transformation.

## V. SUMMARY AND OUTLOOK

In this paper, by considering a class of Pauli stabilizer codes, we constructed a more unified ERG framework through adding/removing more general degrees of freedom. The well-established ERG processes of the 2D toric code and 3D X-cube model are naturally included as the simplest cases. All Pauli stabilizer codes considered here are categorized into a

series of “state towers” as shown in Fig. 1; in each tower, lower LRE states of level- $n$  are added/removed in the level- $n$  ERG process of an upper LRE state of level- $(n + 1)$ . Several future directions are listed below.

First, we may expect a more general ERG framework shown in Eq. (4) can be constructed in other stabilizer codes.

Second, the completeness of the concept of level of LRE states needs further exploration. For example, for type-II fracton ordered states [31, 38], such as Haah’s code [39], a series of ERG transformations have been constructed and studied [23, 24, 26], nevertheless, whether it is possible to consistently assign a level to such Type-II fracton ordered states and corresponding ERG transformations is yet to be determined. Some further discussion about the hierarchy of ERG transformations may be beneficial for a more complete understanding of the entanglement patterns in more generic fracton orders.

Third, except for the stabilizer code models considered in this paper, physically, we can also consider models perturbed by external fields, which are no longer exactly solvable. Constructing ERG transformations for such models to investigate whether they would flow to the fixed points discussed in this paper is also an interesting direction. And some numerical techniques may also be useful in the study of such models [40–42].

Finally, it is known that the ERG transformations are related to MERA, that is a kind of tensor networks capable of efficiently encoding the entanglement signatures of certain quantum many-body states [6–8, 43]. In Ref. [22], it has been noticed that  $[0, 1, 2, 3]$  (X-cube) ground states bear exact branching MERA representations. Then it is natural to ask whether LRE states of general levels can have such tensor network representations. If so, the holographic geometries generated by such tensor networks are also worth exploring [44–46].

## ACKNOWLEDGMENTS

This work was supported by Guangdong Basic and Applied Basic Research Foundation under Grant No. 2020B1515120100 and NSFC Grant No. 12074438.

## Appendix A: A brief introduction of controlled-NOT (CNOT) gate

Here we give a brief introduction of the controlled-NOT (CNOT) gate that is to be frequently used in the main text of this paper.

By definition, CNOT gate is a 2-qubit unitary operation. In  $\sigma^z$  basis, for  $|x\rangle, |y\rangle$ , where  $x, y \in \{0, 1\}$ , CNOT gate maps  $|x\rangle \otimes |y\rangle$  to  $|x\rangle \otimes |y \oplus x\rangle$ , here  $\otimes$  means tensor product,  $\oplus$  means modulo 2 addition. Effectively, CNOT gate regards the first qubit as a *control qubit*, and the second qubit as a *target qubit*. When the control (first) qubit is  $|0\rangle$ , then CNOT gate does nothing; when the control qubit is  $|1\rangle$ , CNOT gate flips the target (second) qubit, thus the name. For example, denoting the action of CNOT gate as  $U$ , we have  $U|01\rangle = |01\rangle$  and  $U|11\rangle = |10\rangle$ .

For the usage in the main text, here we also introduce the conjugate action of CNOT gate on stabilizer generators (i.e., Hamiltonian terms of a stabilizer code model). For a state  $|\phi\rangle$  in the stabilizer subspace and a stabilizer generator  $G$  (i.e.  $G|\phi\rangle = |\phi\rangle$ ), if we apply a CNOT gate  $U$  on  $|\phi\rangle$ , then we have  $(UGU^\dagger)U|\phi\rangle = U|\phi\rangle$ . That is to say, the transformed state  $U|\phi\rangle$  is stabilized by  $UGU^\dagger$ , that is  $G$  acted by the conjugate action of the CNOT gate. For a specific  $G$  acting non-trivially on some control or target qubits, the correspondence between  $G$  and  $UGU^\dagger$  can be expressed as follows[5, 22]:

$$\begin{aligned} ZI &\rightarrow ZI \\ IZ &\leftrightarrow ZZ \\ XI &\leftrightarrow XX \\ IX &\rightarrow IX, \end{aligned}$$

where the first qubit refers to the control qubit, and the second qubit refers to the target qubit. For example, if we consider the conjugate action of a CNOT gate on a stabilizer generator  $G$ , where  $G$  applies a  $\sigma^x$  on the control qubit, and applies an identity on the target qubit, then the corresponding  $UGU^\dagger$  will apply  $\sigma^x$  on both qubits.

## Appendix B: Proof of the equivalence between $H_2$ and $H_3$

In this appendix, we concretely demonstrate that in Sec. IV B, all terms in  $H_3$ , the Hamiltonian of  $[d, d + 1, d + 2, D]$  model on the lattice of the size  $L_1 \times L_2 \times \dots \times (L_D + 1)$  with PBC, can be obtained by taking the product of terms in  $H_2$ , thus they are equivalent stabilizer code models. As we can notice that  $H_2$  and  $H_3$  only have different terms around the  $T^{D-1}$  with  $x_D = 1$ , we only need to consider terms defined on locations with  $0 \leq x_D \leq 2$ .

Before discussing about terms in  $H_2$ , we would like to give a detailed demonstration and classification of the terms around the cut  $T^{D-1}$  in  $H_1 = H_{dddD} + H_{dddD-1} + H_{zz}$ . Such terms in  $H_1$  can be classified as follows:

- *BI* terms:  $B$  terms with  $x_D = 0$  from  $H_{dddD}$  that only involve qubits with  $x_D = 0$ .
- *BII* terms:  $B$  terms with  $x_D = 0$  from  $H_{dddD}$  that simultaneously involve qubits with  $x_D = 0$  and  $x_D = \frac{1}{2}$ .
- *BIII* terms:  $B$  terms with  $x_D = \frac{1}{2}$  from  $H_{dddD}$ .
- *BIV* terms:  $B$  terms with  $x_D = 1$  from  $H_{dddD-1}$  (i.e. such  $B$  terms only involve qubits with  $x_D = 1$ ).
- *BV* terms:  $B$  terms with  $x_D = \frac{3}{2}, 2$  from  $H_{dddD}$ .
- *AI* terms:  $A'_{\gamma_D} = A_{\gamma_D} A_{\gamma_D + I_D}$  terms with  $x_D = \frac{1}{2}$  from  $H_{dddD}$ .
- *AII* terms:  $A_{\gamma_{D-1}}$  terms with  $x_D = 1$  from  $H_{dddD-1}$ .
- *C* terms:  $C_{\gamma_{d+1}} = \sigma_{\gamma_{d+1}}^z \sigma_{\gamma_{d+1} + I_D}^z$  with  $x_D = \frac{1}{2}$  from  $H_{zz}$ .

And we can notice that, around the  $T^{D-1}$ ,  $H_3$  is composed of  $BI$ ,  $BII$ ,  $BIII$ ,  $BIV$ ,  $BV$ , and the following terms:

- $BVI$  terms:  $B$  terms with  $x_D = 1$  that involve qubits with  $x_D \neq 1$ .
- $AIII$  terms:  $A_{\gamma_D}$  terms with  $x_D = \frac{1}{2}, \frac{3}{2}$ .

Then, we consider the conjugate action of the LU transformation  $\mathcal{U}$  on the terms in  $H_1$ , that leads to terms of  $H_2$ :

- A  $BI$  term  $B_{\gamma_d}$  is mapped to  $B_{\gamma_d}B_{\gamma_d+I_D}$ , the product of the  $BI$  term itself and a  $BIV$  term  $B_{\gamma_d+I_D}$ .
- A  $BII$  term  $B_{\gamma_d}$  is mapped to (a) the  $BII$  itself, if the qubits with  $x_D = 0$  and  $x_D = \frac{1}{2}$  in  $B_{\gamma_d}$  are controlled by the same pair of qubits from the  $T^{D-1}$ ; (b)  $B_{\gamma_d}B_{\gamma_d+I_D}$ , the product of the  $BII$  term itself and a  $BIV$  term  $B_{\gamma_d+I_D}$ , if otherwise.
- A  $BIII$  term  $B_{\gamma_d}$  is mapped to (a) the  $B_{\gamma_d}$  itself, if 2 perpendicular qubits in  $B_{\gamma_d}$  (i.e., the 2 qubits are nearest and from different  $(d+1)$ -dimensional subsystems) share 1 control qubit; (b)  $B_{\gamma_d}B_{\gamma_d+I_D}$ , the product of the  $BIII$  term itself and 2  $BIV$  terms  $B_{\gamma_d+I_D}$  and  $B_{\gamma_d+2I_D}$ , if 2 perpendicular qubits in  $B_{\gamma_d}$  have control qubits that nearest to the same  $\gamma_d$ ; (c)  $B_{\gamma_d}B_{\gamma_d+I_D}B_{\gamma_d+2I_D}B_{\gamma_d+3I_D}$ , the

product of the  $BIII$  term itself and 4  $BIV$  terms  $B_{\gamma_d+I_D}$ ,  $B_{\gamma_d+2I_D}$ ,  $B_{\gamma_d+3I_D}$  and  $B_{\gamma_d+4I_D}$ , if otherwise;

- $BIV$ ,  $BV$ ,  $AI$  terms stay invariant.
- An  $AII$  term  $A_{\gamma_{D-1}}$  terms with  $x_D = 1$  is mapped to an  $AIII$  term  $A_{\gamma_D}$  with  $x_D = \frac{1}{2}$ , where the  $\gamma_D$  is obtained as  $\gamma_D = \gamma_{D-1} - \frac{1}{2}I_D$ .
- A  $C$  term  $C_{\gamma_{d+1}}$  term is mapped to a  $BVI$  term  $B_{\gamma_d}$  with  $x_D = 1$ , where the  $\gamma_d$  is obtained as  $\gamma_d = \gamma_{d+1} + \frac{1}{2}I_D$ .

Because  $BIV$ ,  $BV$ ,  $AI$  terms are invariant under the conjugate action of  $\mathcal{U}$  (i.e., they present in  $H_2$ ), we can obtain an arbitrary  $BI$ ,  $BII$  or  $BIII$  term by taking the product of the corresponding transformed term with invariant  $BIV$  terms. An arbitrary  $AIII$  term with  $x_D = \frac{1}{2}$  can be obtained as a transformed  $AII$  term, and an arbitrary  $AIII$  term with  $x_D = \frac{3}{2}$  can be obtained by taking the product of a transformed  $AII$  term and an invariant  $AI$  term. Besides, by taking the product of a transformed  $C$  term with a  $BIV$  terms, an arbitrary  $BVI$  term can also be obtained. Finally, because it is straightforward to check that all terms in  $H_2$  can be obtained by taking products of terms in  $H_3$ , as two stabilizer code models,  $H_2$  and  $H_3$  have equivalent sets of stabilizer generators, thus the stabilizer subspaces should be equivalent.

- 
- [1] Steven R. White, “Density matrix formulation for quantum renormalization groups,” *Phys. Rev. Lett.* **69**, 2863–2866 (1992).
- [2] Steven R. White, “Density-matrix algorithms for quantum renormalization groups,” *Phys. Rev. B* **48**, 10345–10356 (1993).
- [3] U. Schollwöck, “The density-matrix renormalization group,” *Rev. Mod. Phys.* **77**, 259–315 (2005).
- [4] G. Vidal, “Entanglement renormalization,” *Phys. Rev. Lett.* **99**, 220405 (2007).
- [5] Miguel Aguado and Guifré Vidal, “Entanglement Renormalization and Topological Order,” *Phys. Rev. Lett.* **100**, 070404 (2008), arXiv:0712.0348 [cond-mat.str-el].
- [6] G. Vidal, “Class of quantum many-body states that can be efficiently simulated,” *Phys. Rev. Lett.* **101**, 110501 (2008).
- [7] Robert König, Ben W. Reichardt, and Guifré Vidal, “Exact entanglement renormalization for string-net models,” *Phys. Rev. B* **79**, 195123 (2009), arXiv:0806.4583 [cond-mat.str-el].
- [8] G. Evenbly and G. Vidal, “Class of Highly Entangled Many-Body States that can be Efficiently Simulated,” *Phys. Rev. Lett.* **112**, 240502 (2014), arXiv:1210.1895 [quant-ph].
- [9] Xie Chen, Zheng-Cheng Gu, and Xiao-Gang Wen, “Local unitary transformation, long-range quantum entanglement, wave function renormalization, and topological order,” *Phys. Rev. B* **82**, 155138 (2010).
- [10] Michael Levin and Xiao-Gang Wen, “Detecting Topological Order in a Ground State Wave Function,” *Phys. Rev. Lett.* **96**, 110405 (2006), arXiv:cond-mat/0510613 [cond-mat.str-el].
- [11] Hui Li and F. D. M. Haldane, “Entanglement Spectrum as a Generalization of Entanglement Entropy: Identification of Topological Order in Non-Abelian Fractional Quantum Hall Effect States,” *Phys. Rev. Lett.* **101**, 010504 (2008).
- [12] Alexei Kitaev and John Preskill, “Topological Entanglement Entropy,” *Phys. Rev. Lett.* **96**, 110404 (2006), arXiv:hep-th/0510092 [hep-th].
- [13] Frank Pollmann, Ari M. Turner, Erez Berg, and Masaki Oshikawa, “Entanglement spectrum of a topological phase in one dimension,” *Phys. Rev. B* **81**, 064439 (2010).
- [14] Bei Zeng, Xie Chen, Duan-Lu Zhou, Xiao-Gang Wen, *et al.*, *Quantum information meets quantum matter* (Springer, 2019).
- [15] Zheng-Cheng Gu and Xiao-Gang Wen, “Tensor-entanglement-filtering renormalization approach and symmetry-protected topological order,” *Phys. Rev. B* **80**, 155131 (2009).
- [16] Xiao-Gang Wen, “Colloquium: Zoo of quantum-topological phases of matter,” *Rev. Mod. Phys.* **89**, 041004 (2017).
- [17] Steven M Girvin, “Introduction to the fractional quantum hall effect,” in *The quantum Hall effect* (Springer, 2005) pp. 133–162.
- [18] X. G. Wen, “Vacuum degeneracy of chiral spin states in compactified space,” *Phys. Rev. B* **40**, 7387–7390 (1989).
- [19] Alexei Kitaev, “Anyons in an exactly solved model and beyond,” *Ann. Phys.* **321**, 2–111 (2006).
- [20] Alexei Kitaev and Chris Laumann, “Topological phases and quantum computation,” Les Houches Summer School “Exact methods in low-dimensional physics and quantum computing” **89**, 101 (2009).
- [21] Michael A. Levin and Xiao-Gang Wen, “String-net condensation: A physical mechanism for topological phases,” *Phys. Rev. B* **71**, 045110 (2005).
- [22] Wilbur Shirley, Kevin Slagle, Zhenghan Wang, and Xie Chen, “Fracton models on general three-dimensional manifolds,” *Phys. Rev. X* **8**, 031051 (2018).

- [23] Jeongwan Haah, “Bifurcation in entanglement renormalization group flow of a gapped spin model,” *Phys. Rev. B* **89**, 075119 (2014), arXiv:1310.4507 [cond-mat.str-el].
- [24] Brian Swingle and John McGreevy, “Renormalization group constructions of topological quantum liquids and beyond,” *Phys. Rev. B* **93**, 045127 (2016).
- [25] Brian Swingle and John McGreevy, “Mixed s -sourcery: Building many-body states using bubbles of nothing,” *Phys. Rev. B* **94**, 155125 (2016), arXiv:1607.05753 [cond-mat.str-el].
- [26] Arpit Dua, Pratyush Sarkar, Dominic J. Williamson, and Meng Cheng, “Bifurcating entanglement-renormalization group flows of fracton stabilizer models,” *Phys. Rev. Research* **2**, 033021 (2020).
- [27] Xiao-Gang Wen, “Systematic construction of gapped nonliquid states,” *Phys. Rev. Research* **2**, 033300 (2020).
- [28] Juven Wang, “Nonliquid cellular states: Gluing gauge-higher-symmetry-breaking versus gauge-higher-symmetry-extension interfacial defects,” *Phys. Rev. Research* **4**, 023258 (2022).
- [29] Rahul M. Nandkishore and Michael Hermele, “Fractons,” *Annu. Rev. Condens. Matter Phys.* **10**, 295–313 (2019).
- [30] Michael Pretko, Xie Chen, and Yizhi You, “Fracton phases of matter,” *International Journal of Modern Physics A* **35**, 2030003 (2020), arXiv:2001.01722 [cond-mat.str-el].
- [31] Sagar Vijay, Jeongwan Haah, and Liang Fu, “Fracton topological order, generalized lattice gauge theory, and duality,” *Phys. Rev. B* **94**, 235157 (2016).
- [32] Meng-Yuan Li and Peng Ye, “Fracton physics of spatially extended excitations,” *Phys. Rev. B* **101**, 245134 (2020).
- [33] Meng-Yuan Li and Peng Ye, “Fracton physics of spatially extended excitations. II. Polynomial ground state degeneracy of exactly solvable models,” *Phys. Rev. B* **104**, 235127 (2021).
- [34] Daniel Gottesman, *Stabilizer codes and quantum error correction*, Ph.D. thesis, California Institute of Technology (1997).
- [35] Alioscia Hamma, Paolo Zanardi, and Xiao-Gang Wen, “String and membrane condensation on three-dimensional lattices,” *Phys. Rev. B* **72**, 035307 (2005).
- [36] Abhinav Prem, Sheng-Jie Huang, Hao Song, and Michael Hermele, “Cage-net fracton models,” *Phys. Rev. X* **9**, 021010 (2019).
- [37] Liang Kong, Yin Tian, and Zhi-Hao Zhang, “Defects in the 3-dimensional toric code model form a braided fusion 2-category,” *Journal of High Energy Physics* **2020**, 78 (2020), arXiv:2009.06564 [cond-mat.str-el].
- [38] Sagar Vijay, Jeongwan Haah, and Liang Fu, “A new kind of topological quantum order: A dimensional hierarchy of quasiparticles built from stationary excitations,” *Phys. Rev. B* **92**, 235136 (2015).
- [39] Jeongwan Haah, “Local stabilizer codes in three dimensions without string logical operators,” *Phys. Rev. A* **83**, 042330 (2011).
- [40] M. Mühlhauser, M. R. Walther, D. A. Reiss, and K. P. Schmidt, “Quantum robustness of fracton phases,” *Phys. Rev. B* **101**, 054426 (2020).
- [41] Chengkang Zhou, Meng-Yuan Li, Zheng Yan, Peng Ye, and Zi Yang Meng, “Evolution of dynamical signature in the X-cube fracton topological order,” *Physical Review Research* **4**, 033111 (2022), arXiv:2203.13274 [cond-mat.str-el].
- [42] Guo-Yi Zhu, Ji-Yao Chen, Peng Ye, and Simon Trebst, “Topological fracton quantum phase transitions by tuning exact tensor network states,” arXiv e-prints, arXiv:2203.00015 (2022), arXiv:2203.00015 [cond-mat.str-el].
- [43] G. Evenbly and G. Vidal, “Scaling of entanglement entropy in the (branching) multiscale entanglement renormalization ansatz,” *Phys. Rev. B* **89**, 235113 (2014).
- [44] G. Evenbly and G. Vidal, “Tensor Network States and Geometry,” *Journal of Statistical Physics* **145**, 891–918 (2011), arXiv:1106.1082 [quant-ph].
- [45] Brian Swingle, “Entanglement renormalization and holography,” *Phys. Rev. D* **86**, 065007 (2012), arXiv:0905.1317 [cond-mat.str-el].
- [46] Glen Evenbly, “Hyperinvariant Tensor Networks and Holography,” *Phys. Rev. Lett.* **119**, 141602 (2017), arXiv:1704.04229 [quant-ph].